Université du Québec
à Rimouski

Étude CFD du système de ventilation d'une chambre d'hôpital pour réduire les infections et atteindre le confort thermique

Mémoire présenté

dans le cadre du programme de maîtrise en ingénierie

en vue de l'obtention du grade maître ès sciences appliquées (M. Sc. A.)

PAR

© Mustafa Alkhalaf

Novembre 2022

Composition du jury :

Véronique Dassylva-Raymond, président du jury, UQAR

Adrian Ilinca, directeur de recherche, UQAR

Mohamed Yasser Hayyani, codirecteur de recherche, UQAR

Khaled Esteifi, examinateur externe, Université d'Alep

Dépôt initial le 9 novembre 2022 Dépôt final le 7 décembre 2022

ACKNOWLEDGMENT

I want to extend my deepest gratitude to my supervisor, Pr. Ilinca Adrian, of noble character, for the support and guidance he provided and my acceptance as one of the master's students on his team.

In addition, I would like to mention Pr. Hayyani Mohamed Yasser, for all the guidance, support, and outstanding feedback.

I am extending my thanks to Pr. Khaled Esteifi, for accepting to participate as a jury member. Your encouragement during my undergraduate studies motivated me to start this research work.

My most profound appreciation to my family, my great father and mother, and my wonderful brothers & sisters, for providing me with unfailing support and continuous encouragement throughout my years of study. This accomplishment would not have been possible without them.

I thank my friends and UQAR University, all the colleagues and employees of this wonderful university, which pays special attention to science and students.

Thank you very much.

RÉSUMÉ

Dans la conception des bâtiments modernes, les systèmes de climatisation occupent un rôle central. Les systèmes de climatisation sont conçus en tenant compte des deux exigences essentielles aux habitats humains : le confort thermique et la qualité de l'air. Satisfaire ces deux exigences devient de plus en plus difficile surtout dans le contexte de nombreuses maladies aéroportées telles que la SARS-Covid-19.

Le but de cette recherche numérique est de simuler différentes conceptions de ventilation avec trois débits 9, 12, et 15 ACH (nombre de changements d'air par heure) pour un modèle de chambre d'hôpital, tout en tenant compte des recherches antérieures. L'objectif ici est d'illustrer comment le réglage du débit d'air et le placement des diffuseurs peuvent affecter le confort thermique et l'élimination des polluants contenant principalement le dioxyde de carbone. Les équations de RANS (Reynolds Averaged Navier Stokes) avec le modèle de turbulence $k - \varepsilon$, ont été utilisées comme modèle mathématique pour le flux d'air. Les conditions aux limites ont été extraites des références de ventilation de l'ASHRAE (American Society of Heating, Refrigerating, and Air-Conditioning Engineers Society) et des études antérieures.

Contrairement à la croyance populaire, les données ont montré que l'augmentation de la ventilation n'améliorait pas nécessairement la distribution de l'air ou n'éliminait pas plus de polluants. L'élimination des polluants est fortement affectée par l'emplacement de l'exutoire. Selon le confort thermique, il existe une corrélation entre le débit d'air, la position de l'entrée et l'intensité de la turbulence. Il a été constaté que le cas à débit 9 ACH et le cas à débit 12 ACH présentaient la meilleure élimination des polluants. De plus, le confort thermique obtenu dans les deux derniers cas était le meilleur parmi les cas étudiés même si

la cible n’a pas été atteinte. Il est à noter que pour ces deux cas, la sortie est située sous le niveau de la tête du patient, et l'air est introduit près du plafond sur le mur opposé.

Mots clés : [Confort thermique, Qualité de l'air, Simulation CFD, Chambre d'isolement, Élimination des contaminants]

ABSTRACT

The main requirement in designing air conditioning systems is to provide thermal comfort to occupants. In addition, the elimination of pollution is one of the crucial health elements in building design, particularly in the presence of many airborne diseases such as Covid-19 lately.

The purpose of this numerical research is to simulate various ventilation designs for a hospital room model by taking into account results obtained by previous researchers. Four designs with three flow rates 9, 12, and 15 ACH (Air Change per Hour), were applied to each. The objective is to determine the effect of airflow and the diffuser location distribution on the thermal comfort and pollutants elimination represented by carbon dioxide. Through SolidWorks Flow Simulation software, Reynold Averaged Navier Stokes (RANS) equations, along with the $k-\varepsilon$ turbulence model are used as the underlying mathematical model for the airflow. In addition, boundary conditions are extracted from ASHRAE (American Society of Heating, Refrigerating, and Air-Conditioning Engineers Society) ventilation publications and from relevant literature.

Contrary to popular belief, the results of this study have demonstrated that the increase in ventilation does not necessarily improve air distribution or remove more contaminants. In addition, pollutant removal has been significantly affected by the outlet's location. Furthermore, a correlation has been deduced for thermal comfort between airflow, diffuser locations, and turbulence intensity. It has been found that case four at flow 9 ACH and case five at flow 12 ACH had the optimum removal of the contaminants. Although thermal comfort is not totally achieved inside the room, still the latter two cases are the best of the 12 cases. It is noteworthy to mention that for these two cases, the outlet is located below the level of the patient's head, and the air is supplied near the ceiling on the opposite wall. However, thermal comfort has not been entirely achieved in the occupied area too.

Keywords: [Thermal Comfort, Air Quality, CFD Simulation, Isolation Room, Contaminant Removal]

TABLE OF CONTENTS

LIST OF TABLES

LIST OF FIGURES

LIST OF ABBREVIATIONS, ABBREVIATIONS, AND ACRONYMS

ACE	Air Exchange Efficiency
ACH	Air Changes per Hour
AIIR	Airborne Infection Isolation Rooms
ASHRAE	The American Society of Heating, Refrigerating, and Air-Conditioning Engineers Society
CFD	Computational Fluid Dynamic
CO_2	Carbon Dioxide
CRE	Contaminant Removal Efficiency
HCW	Health Care Worker
HVAC	Heating Ventilation Air Conditioning System
IAQ	INDOOR AIR QUALITY
IEA	International Energy Agency
LEV	Local Exhaust Ventilation
PMV	Predicted Mean Vote
PPD	Predicted Percent Dissatisfied
SARS	Severe acute respiratory syndrome
VOCs	Volatile Organic Compounds

LIST OF SYMBOLS

$\mathbf{u}$	the fluid velocity	m/s
$\boldsymbol{\rho}$	the fluid density	Kg/m3
$\boldsymbol{S_i}$	the mass-distributed external force	
$\boldsymbol{S_i^{gravity}}$	the buoyancy	Newton
$\boldsymbol{g_i}$	gravitational acceleration	m/s^2
$\boldsymbol{S_i^{rotation}}$	the coordinate system's rotation	
$\boldsymbol{h}$	the thermal enthalpy	Joule
$\boldsymbol{Q_H}$	the heat source or sink per unit volume	$J/K{\cdot}m^3$
$\boldsymbol{\tau_{ij}}$	the viscous shear stress tensor	
$\boldsymbol{q_i}$	the diffusive heat fluxes	w/m^3
$\boldsymbol{\Omega}$	the angular velocity of the coordinate system in rotation	rad/s
$\boldsymbol{r}$	the distance between a point and the axis of rotation in the frame of rotation	m
$\boldsymbol{k}$	the kinetic energy of the turbulence	J/kg
$\boldsymbol{h_m^0}$	the individual thermal enthalpy	Joule
$\boldsymbol{y_m}$	the concentration of the m-th component of the mixture	mol/m^3

$\boldsymbol{\delta_{ij}}$	the Kronecker delta function	
$\boldsymbol{\mu}$	the dynamic viscosity parameter	Pa-s
$\boldsymbol{\mu_t}$	the turbulent eddy viscosity coefficient	kg/m-s
$\boldsymbol{k}$	the turbulent kinetic energy	J/kg
$\boldsymbol{f_\mu}$	the turbulent viscosity factors	m^2/s
$\boldsymbol{y}$	the distance to the wall	m
$\boldsymbol{P_B}$	the turbulent generation due to buoyancy forces	
$\boldsymbol{Le}$	the Lewis numbers	
$\boldsymbol{Pr}$	the Prandtl number	
$\boldsymbol{h}$	the enthalpy	Joule
$\boldsymbol{p}$	the static pressure of the carrier fluid	pascal
$\boldsymbol{R}$	the universal constant of the gas	J /K-mol
$\boldsymbol{m}$	the carrier fluid and the molar mass of the mixture of the substance	
$\boldsymbol{m_1}$	the molar mass of the substance	Kg /mol
$\boldsymbol{m_2}$	the molar mass of the carrier fluid	Kg /mol
$\boldsymbol{v_1}$	the specific volume of the substance	m 3 /kg
$\boldsymbol{\mu}$	the laminar viscosity of the carrier fluid	Pa-s
$\boldsymbol{\mu_t}$	the turbulent viscosity of the carrier fluid	m^2/s

$\boldsymbol{Pr}$	the laminar Prandtl numbers of the carrier fluid,	
$\boldsymbol{Pr_t}$	the turbulent Prandtl numbers of the carrier fluid,	
$\mathbf{L_e}$	the laminar Lewis numbers of the carrier fluid	
$\mathbf{Le_t}$	the turbulent Lewis numbers of the carrier fluid	
$\boldsymbol{V}$	the fluid volume of the computational domain	m^3
$\boldsymbol{Q}$	the volume flow rate of air entering that fluid volume.	l/s
$\boldsymbol{C}$	the mass fraction of the contamination at a specific point.	ppm
$\boldsymbol{C_e}$	the average fraction of mass to the contaminant.	ppm
$\boldsymbol{M}$	the metabolic rate	J /s
$\mathbf{W}$	the external work	J
$\boldsymbol{I_{cl}}$	the thermal resistance of the clothes	K/W
$\boldsymbol{f_{cl}}$	the ratio of the dressed surface to the bare surface	
$\boldsymbol{T_a}$	the air temperature	K
$\boldsymbol{T_r}$	the mean radiant temperature	K
$\boldsymbol{V}$	the relative air velocity	m /s
$\boldsymbol{P_a}$	the partial pressure of water vapor	pascal
$\boldsymbol{h_c}$	the convective heat transfer coefficient	$W/(m^{2\cdot} K)$
$\boldsymbol{T_{cl}}$	the surface temperature of the garment	K

GENERAL INTRODUCTION

The coronavirus pandemic has resulted in more than 15 million infections and over 619,000 deaths worldwide in 2020. The regions most affected by the pandemic are Asia, particularly China, Europe, the United States, South America, and Mexico. Severe acute respiratory syndrome (SARS-CoV-2) can spread over long distances through the air. Therefore, airborne transmission played a significant role in the rapid propagation of the SARS epidemic (Borro *et al*., 2021). Given the rapid spread of the disease, hospitals are compelled to treat patients in isolation. When an infected individual sneezes or coughs, microscopic particles are disseminated throughout the environment. If another person inhales these particles, he may get sick. Therefore, airborne infectious diseases can rapidly spread in an inadequately ventilated isolation room. Rooms with a proper ventilation system will be free of any infectious airborne particles, such as viruses, bacteria, or microorganisms (Hallé, 2016) & (Anuraghava *et al*., 2021).

Furthermore, thermal comfort has been the subject of many studies over the last few years. Sensing, controlling, and predicting indoor air quality should be monitored for thermal comfort. Patients in social facilities spend 80-90% of their time indoors. Hence, it is required to provide appropriate humidity, and temperature should also be considered as a significant factor. Additionally, creating a relaxing atmosphere for them can aid in their recovery rapidly (Akili *et al*., 2021). Academic scientists and industrial engineers are trying to explore the finest ways to improve the design of hospital wards by controlling the temperature, humidity, contaminants, and velocity of the supplied air, along with modifying the diffuser's locations (*HVAC DESIGN MANUAL FOR HOSPITALS AND CLINICS*, 2012).

CHAPTER 1 BACKGROUND

1.1 THERMAL COMFORT

The American Society of Heating, Refrigerating, and Air-Conditioning Engineers has defined thermal comfort as “The condition of the mind in which satisfaction is expressed to the existing environment” (*Thermal Environmental Conditions for Human Occupancy*, 2004). Thermal comfort has been the subject of intense research over the years.

Below are several key indicator factors used to estimate the ventilation system's effectiveness in thermal comfort in the conditioned area.

Draft Temperature can be defined as “the difference in temperature between any two points in the occupied zone and the control condition.” *"Draft"* is defined as any localized feeling of coolness or warmth of any portion of the body due to air movement and air temperature, with humidity and radiation considered as constant.

Predicted Mean Vote (PMV) is an index that predicts the mean value of the votes of a large group of people. Based on the heat balance of the human body, where the thermal balance is obtained when the internal heat production in the body is equal to the heat loss to the environment**.**

Predicted Percent Dissatisfied (PPD) “is information that provides about thermal discomfort or thermal dissatisfaction by predicting the percentage of people likely to feel warm or cool in a given environment” (*TUTORIALS SOLIDWORKS FLOW SIMULATION 201*, 2021).

1.2 INDOOR AIR QUALITY (IAQ)

During the ventilation system operation, the occupants' attention is focused on thermal comfort because the sensation of thermal comfort is immediate and thermal discomfort cannot be tolerated. However, poor air quality is hard to notice, so the occupants' response takes longer. (*Novoselac_ASHRAE_Transactions_2003*, 2003). Obtaining efficient ventilation, indoor air quality (IAQ) is essential for human health, productivity, and well-being. For instance, a good IAQ includes effectively removing indoor pollutants and adequate fresh outdoor air for occupants (Tian *et al*., 2020). Several indicators assess ventilation efficiency.

Contaminant removal efficiency (CRE) and air exchange efficiency (ACE) are widely used indicators because they can be easily measured in the field or the laboratory and applied to all ventilation methods. In addition, they are generic, and almost all other indicators are extensions of them. For example, CRE is an indicator of the pollution level in a room that depends not only on the airflow pattern but also on the characteristics of pollutant sources, such as density, area, and positions (*Novoselac_ASHRAE_Transactions_2003*, 2003).

IAQ can be assessed in terms of the concentration of gaseous ingredients. Many gaseous ingredients such as Volatile Organic Compounds (VOCs), formaldehyde, nitrogen oxides, sulfur oxide, carbon dioxide, carbon monoxide, particulates, and infectious pollutants often degrade indoor air quality. The high concentration of these pollutants leads to serious health effects and inconvenience for patients. Pollutants other than carbon dioxide are usually recorded as sufficiently below the standard limit (Daisey *et al*., 2003). In addition, the carbon dioxide concentration depends on the number of humans inside an occupied space. Therefore, carbon dioxide concentration is widely used as an indicator of IAQ.

1.3 VENTILATION STRATEGIES

No sole ventilation design solution can solve all the airborne transferable particle concentration problems and consistently be cost-effective. Therefore, ventilation designers must always consider the cost of installing and operating their systems and need effective control strategies for air systems to make a feasible design (American Society of Heating, 2012). Therefore, various healthcare facility ventilation designs provide a minimum ventilation equivalent to 12 ACH for isolation rooms (Bolashikov *et al*., 2012).

According to (Chow *et al*., 2006), the transmission of air pollutants has the potential to spread disease to healthcare workers and patients.

The pressure value of the air inside a hospital room should be checked and adjusted correctly accordingly to its usage. For example, if the room is host to a transmissible disease, the room's pressure is lowered to prevent particles from leaking out of the room; if the room is used for an operation, the room's pressure is increased to prevent particles from entering so the space can be kept sterile (Alhamid *et al*., 2018). Therefore, for the systems serving Airborne Infection Isolation Rooms (AIIR), negative air pressure must be designed relative to adjacent rooms or hallways. However, an AIIR plan with negative pressure involves a complex decision-making process (Cho, 2019).

Several studies have noted an interdependence between ventilation and health, but the actual relationship and attributable mechanisms remain unclear. In addition, the data was insufficient to define minimum ventilation standards to control the prevalence of airborne disease in any setting. Consequently, it revealed the uncertainty about the connection between ventilation and health (Mousavi, 2015).

1.4 DIFFUSERS LOCATIONS

The airflow direction depends on the room pressure and the inlet/outlet distribution through the space. Accordingly, a cautious and intentional ventilation device can be more effective in containing and removing airborne contaminants (Mousavi, 2015). Unfortunately, the literature does not provide enough indication of the location of outlets and inlets. For example, it does not limit the maximum and minimum distances between the two openings (Abdel & Saadeddin, 2016). As per ASHRAE standards, space air diffusion has defined some particular rules, trying to guide the designers toward the best design. For example, it mentions that the outlet diffuser should be located between the supply diffuser or on the side of the room away from the supply diffuser, to reduce short-circuiting of supplied air (Abdel & Saadeddin, 2016).

Moreover, to organize the airflow pattern, standards and guidelines have been provided by ASHRAE for all aspects of the system's design. The medium's temperature distribution primarily determines human comfort because that's how the body's metabolic heat is dissipated into the surrounding air. Therefore, a stagnant layer of ambient air must be created to maintain intake velocities and temperatures within a specified comfort range. It is always advisable to keep the stagnation layer above the occupied cooling zone and as close to the ground as possible in case of heating (*Engineering Guide Air Distribution*, 2011).

1.5 OBJECTIVE

The primary goal of this research is to conduct a numerical study of several ventilation system strategies for a hospital isolation room. This study focuses on determining the optimum strategy to protect healthcare workers from being inoculated and to eliminate infectious sources or, at least, reduce their spread. Furthermore, the objective of the present study also includes checking the degrees of the temperature gradient across the room to achieve comfort inside the conditioned space.

The specific objectives are:

- Choosing an appropriate geometrical and mathematical model along with a numerical method for simulating airflow and CO_2 dynamic behavior in a three-dimensional (3D) room.
- Propose different flow patterns and ventilation scenarios to be analyzed and investigated.
- Demonstrate the results of simulating thermal comfort, pollutants concentration, and airborne particle distribution for various designs.

CHAPTER 2
LITERATURE REVIEW

A numerical study was conducted by Thatiparti *et al*. (2017), to determine the effect of the distribution of air vents on the possible flow path of contaminant spread in an isolation room. It was found that the exhaust has little impact on the removal of coughing aerosols (contaminants) at 12 ACH, except for those in high-impact areas, such as near the exhaust grille in a high-speed region.

Researchers from Johns Hopkins University (Therkorn *et al*., 2019) completed a numerical study through vaporized fluorescent molecules to explore the leakage rate when the exhaust failed and designed an automated air conditioning system that increased airflow to adjacent areas of the isolation rooms. They found that, in case of a failure of the air conditioning systems, 6% of the fluorescent particles were transported through the cracks around the doors/door handles outside the isolation room through the air flow alone and not by the movement of individuals or doors, which indicate the importance of exhaust.

The comparison of the efficiency of three ventilation systems, using computational fluid dynamics modeling and field measurement, has been reported in a study by Cho (2019). The study aimed to protect healthcare workers from the spread of airborne infectious diseases caused by patients' contaminated exhaled air in a negative-pressure isolation room. The observations and simulation results from three ventilation systems are used to propose a new ventilation strategy for isolation rooms, which is the most effective in eliminating contaminants. The findings demonstrate the superiority of ventilation systems that employ the "low-level extraction" method for eliminating pollutants in the breathing zone of humans.

The air change rate and efficiency of pollutant removal were used to assess AIIR ventilation performance in three Finnish hospitals (Kekkonen *et al*., 2014). The results showed that the AIIR's and anteroom's high ventilation rates (4 – 24) ACH were insufficient to stop the spread of infectious microorganisms due to improper airflow.

Researchers at the University of Cordoba (Villafruela *et al*., 2019) conducted an experimental and numerical study to assess ventilation at three different rates of air change of 6,9 and 12 ACH in the transport of pollutants to a patient (P) lying in a hospital bed to a healthcare worker (HCW) standing beside the bed. They found that increasing ACH cannot reduce exposure and, in some circumstances, may increase it.

Another numerical study (Yam *et al*., 2011) aimed to recognize the role of ventilation in preventing and controlling infection in general hospital wards and obtain a simple design, cost-effective ventilation system to reduce infection. The study's results revealed that rearranging the air return diffuser position and increasing the aeration rate to 12 ACH kept the ventilation under control and enhanced its ability to reduce the risk of transmitting diseases to public wards.

A series of experimental and numerical tests were performed (Mousavi & Grosskopf, 2014) in a hospital to monitor the containment and removal of inhalable aerosols 0.5-10 μm concerning the ventilation rate in the isolation room. It was found that increased ventilation from 2.5 to 5.5 ACH resulted in reducing aerosol concentrations by only 30%. Higher ventilation rates were not relatively effective in reducing the concentration of pollutants.

In his Ph.D. thesis, Mousavi (2015), reviewed the spatial and temporal movement of aerosols from the global ventilation system of the hospital and assessed the possibility of contamination from infectious sources within isolation rooms and adjacent corridors. It was concluded that a proper arrangement of the vents could reduce concentrations and improve particulate removal.

To assess the ventilation system in hospital spaces, Balocco & Lio (2011), considered a full-scale isolation room prepared in Tuscany, Italy. They investigated the temporal

dynamics of the ventilation flow and the particle tracing in the conditions of coughing and breathing for two patients. The study was performed using 3D models. Simulation results of the ventilation path and air distribution indicate that the air supply in the ceiling results in variable-direction air flows. Furthermore, the flow in the region between the three opposite air return diffusers interacts with the unstable local flows, causing the production of a low-pressure area that drags up some recirculation air.

A numerical computational fluid dynamics (CFD) approach is applied by Lu *et al*. (2020), to investigate if the representation of CO_2 could be achieved and explore contaminant distribution in a two-bed hospital ward with two patients and one healthcare worker under different types of ventilation. For simulating the exhaled and coughed contaminants by patients with different postures, a tracer gas (CO_2) is applied. The results demonstrate that stratum ventilation minimizes the exposure risk of healthcare workers in hospital wards. Furthermore, under stratum ventilation, the contaminant concentration in the breathing zone at 1.3–1.7 m above the floor is lower, and the contaminant removal effectiveness is comparably higher.

To determine the importance of the role of the air outlet near the patient, Borro *et al*. (2021), were investigated the role of HVAC systems in the spread of infection through computational fluid dynamics (CFD) simulation cough at Bambino Gesu Children's Hospital in the Vatican State. In addition, the potential role of exhaust ventilation systems placed over the mouth of a coughing patient was also assessed. Despite doubling the airflow in the HVAC system providing a significant reduction in the concentration of airborne pollutants, it also results in a significant increase in turbulent air movement, which gives the droplets and air pollutants a spread of increased and faster long-range in the room. However, the presence of the Local exhaust ventilation (LEV) unit above the patient's face illustrates a very high capacity to reduce droplets and polluted air in the room, guaranteeing the total absence of exposure to infection risks for the patient.

The thermal comfort of an office located in the city center of Krakow (southern Poland) was studied by Borowski *et al*. (2021), to demonstrate the air distribution parameters of the

supply air diffuser. Tests were carried out on two longitudinal with different types of diffusers, with nozzles and adjustable nozzles, which were part of the office's air conditioning system. It was found that the microclimate of a particular room and the comfort conditions also depend on the room's air velocity, not only on the temperature and humidity values, especially in the occupied zone. In addition, incorrect selection of the type or location of air conditioning system components can contribute to local discomfort for building occupants.

SolidWorks software was used to develop a 3D digital simulation for predicting human comfort levels. Prabhakaran *et al*. (2018), added the heat source model to ventilation to assess human comfort factors and indoor air temperature. Net person's heat load, coolant heat source, and solar radiation are considered. The results of the PMV and PPD indicators are very reasonable values compared to existing research on human comfort levels compared to (ASHRAE).

Another study (Ahmed, 2012) studied the ventilation system's performance in a typical hospital room using SolidWorks flow simulation software. Achieving indoor air quality (IAQ) depends on many factors, including removing pollutants. Therefore, CRE greater than one is strongly required for the optimal ventilation system. The simulation gives a CRE of 1.23 for exhaled air, which means that the ventilation system is reasonably efficient in removing polluted air, although the study result was satisfactory. However, the results obtained through this study are not blindly applicable to hot and humid countries.

Another research (Ameer *et al*., 2021) examines how social distance works in ventilated interior environments. The role of airflow in dispersing airborne viral diseases has been studied with the help of Computational Fluid Dynamics software (SolidWorks). Increasing the flow rate of the outlet leads to a greater CRE value. A more significant flow velocity at the outlets will be more effective in excreting out the pollutant, which is still present inside the place.

Anuraghava *et al*. (2021), have investigated the importance of negative pressure and the flow diffuser pattern by computational fluid dynamics simulations to verify the spread of

airborne viruses inside a negative pressure room with a mixed-mode ventilation system. The results are effective in the negative pressure room as the particles are brought together and directed to the outlet without diffusion into the space. This was observed for the different-sized particles, and also, it was found that there was no significant difference in the flow patterns.

When it comes to eliminating air contaminants inside the building, conventional mixing ventilation is inefficient. Cheng *et al*. (2021), looked into how a localized laminar airflow ventilation system can reduce the transmission of contaminants. Thermal breathing manikins were employed in both the seated and supine positions. Based on the results of this research, a localized laminar airflow ventilation system may effectively deliver clean air to the breathing zone without negatively impacting the ambient temperature.

Airflow and temperature distributions by Pulat & Ersan (2015), in the International Energy Agency (IEA) chamber, were predicted to investigate the effects of inlet turbulence intensity and length scale on flow characteristics because of the multiplicity of solutions. The validated turbulence model is then used to verify the effects of turbulence intensity and length scale. The results revealed that the length scale difference does not affect the flow pattern at a low value of inlet turbulence intensity (Tu = 0.01). Furthermore, the increase in turbulence intensity has no effect on the flow pattern at a constant high-length scale value at a high inlet turbulence intensity value (Tu = 0.4). While for constant low and middle-length scale values, an increase in inlet turbulence intensity from 0.01 to 0.4 affects the flow pattern.

In this research (Croitoru *et al*., 2011), several ventilation strategies were tested to evaluate the thermal comfort of the occupants and aimed to assess the effect of several flow parameters: the intensity of turbulence at the inlet of air diffusers and the local sensation of thermal discomfort for ventilation users. Local correlations have been found between turbulence intensity and body convective heat flux. However, the heat fluxes exchanged between the different body parts and their environment vary significantly between the cases studied. The PMV and PPD indices seem less sensitive to the local disturbance severity value.

The conclusion for the previous studies is as follows:

Previous studies have not clarified the diffuser's location and role in containing pollutants. Some believe that the location has a minimal impact on the outcomes (parameters), while others found that the location is considered a significant factor. From the literature survey, it has become apparent that the arrangement of diffusers has a significant impact, which can be either positive or negative, and the ventilation rate could determine that.

Concerning the required value of airflow, previous researchers have tried to establish an interval. However, even the standards have varying recommendations and are not precisely defined. Some suggested that increasing the ventilation to a specific limit reduces the pollutant's concentration, which reduces exposure to it. In contrast, few studies indicated that increasing the airflow has a negative effect because it makes the contamination spread all over the room.

CHAPTER 3

METHODOLOGY AND MATHEMATICAL MODEL

This chapter discusses the significance of CFD in modeling ventilation systems in an enclosed space, and it also discusses the turbulence model and the gas diffusion equation. The source of the pollutants (breathing) is represented by carbon dioxide. In addition, thermal comfort equations, isolation room design, boundary conditions, and mesh setting were included in the analysis of the current study.

3.1 GOVERNING EQUATIONS

Computational Fluid Dynamics (CFD) is the most advanced building simulation method based on Naiver Stokes equations to solve the flow field in the fluid domain inside the building (Risberg, 2018). CFD is used in this study as a computational tool for numerical simulations, as it includes modeling by formulating a mathematical physics problem. Numerical methods are used to solve the problem by the estimation methods' resolution of numerical parameters through specific equations (Ghanta, 2020).

3.1.1 Turbulence model

Reynolds number is the product of representative velocity and length scales divided by kinematic viscosity and characterizes laminar and turbulent flows. Most of the fluid flows encountered in engineering practice are considered turbulent, so flow simulations were mainly developed to simulate and study turbulent flows. Average Favre-Navier-Stokes

equations are used to predict turbulent flows, in which the effects of time-averaged flow turbulence on flow parameters are considered.

The general laws of mass, angular momentum, and energy conservation can be written in a cartesian frame rotating at an angular speed Ω around an axis passing through the origin of the frame in the following conservation form (SOLIDWORKS FLOW SIMULATION, 2021):

$$\frac{\partial \rho}{\partial t} + \frac{\partial}{\partial x_i}(\rho u_i) = 0 \tag{3.1}$$

$$\frac{\partial \rho u_i}{\partial t} + \frac{\partial}{\partial x_i}(\rho u_i u_j) + \frac{\partial p}{\partial x_i} = \frac{\partial}{\partial x_i}(\tau_{ij} + \tau_{ij}^R) + S_i \quad ; i = 1,2,3 \tag{3.2}$$

$$\frac{\partial \rho H}{\partial t} + \frac{\partial \rho u_i H}{\partial x_i} = \frac{\partial}{\partial x_i}\left(u_j(\tau_{ij} + \tau_{ij}^R) + q_i\right) + \frac{\partial p}{\partial t} - \tau_{ij}^R \frac{\partial u_i}{\partial x_j} + \rho\varepsilon + S_i u_i + Q_H, \tag{3.3}$$

$$H = h + \frac{u^2}{2} + \frac{5}{3}k - \frac{\Omega^2 r^2}{2} - \sum_m h_m^0 y_m, \tag{3.4}$$

Where u is the fluid velocity, ρ is the fluid density, S_i is a mass-distributed external force per unit mass due to a porous media resistance (S_i^{porous}), a buoyancy $\left(S_i^{gravity} = -\rho g_i\right)$, where g_i is the gravitational acceleration component along the i-th coordinate direction, and the coordinate system's rotation ($S_i^{rotation}$), i.e., $S_i = (S_i^{porous} + S_i^{gravity} + S_i^{rotation}$, h is the thermal enthalpy, Q_H is a heat source or sink per unit volume, τ_{ij} is the viscous shear stress tensor, q_i is the diffusive heat flux, Ω is the angular velocity of the coordinate system in rotation, r is the distance between a point and the axis of rotation in the frame of rotation, k is the kinetic energy of the turbulence, h_m^0 is an individual thermal enthalpy of the m-th component of the mixture, y_m is a concentration of the m-th component of the mixture. Subscripts are used to indicate grouping across the three coordinate directions. In this study, there is no rotation of the flow domain and no porous media resistance. Therefore, those terms are set to zero in the simulations.

The viscous shear tensor for Newtonian fluids is defined as:

$$\tau_{ij} = \mu\left(\frac{\partial u_i}{\partial x_j} + \frac{\partial u_j}{\partial x_i} - \frac{2}{3}\delta_{ij}\frac{\partial u_k}{\partial x_k}\right) \quad 3.5$$

The Reynolds-stress tensor as the following Boussinesq assumption has the following form:

$$\tau_{ij}^R = \mu_t\left(\frac{\partial u_i}{\partial x_j} + \frac{\partial u_j}{\partial x_i} - \frac{2}{3}\delta_{ij}\frac{\partial u_k}{\partial x_k}\right) - \frac{2}{3}\rho k\delta_{ij} \quad 3.6$$

Here is δ_{ij} the Kronecker delta function (it is equal to unity when $i = j$, and zero otherwise), μ is the dynamic viscosity parameter, μ_t is the turbulent eddy viscosity coefficient and k is the turbulent kinetic energy. Note that μ_t and k are zero for laminar flows. Within k-ε turbulence model, μ_t is defined using two basic turbulence properties, namely, the turbulent dissipation ε and the turbulent kinetic energy k.

$$\mu_t = f_\mu \frac{C_\mu \rho k^2}{\varepsilon} \quad 3.7$$

Here f_μ is a turbulent viscosity factor. It is defined by the expression

$$f_\mu = \left[1 - \exp\left(-0.0165R_y\right)\right]^2 \times \left(1 + \frac{20.5}{R_T}\right), \quad 3.8$$

Where: $R_T = \frac{\rho k^2}{\mu\varepsilon}$, $R_y = \frac{\rho\sqrt{k}y}{\mu}$, $with\ y$, is the distance to the wall. This function makes it possible to take into account the laminar-turbulent transition. Two additional transport equations are used to describe turbulent kinetic energy and dissipation,

$$\frac{\partial \rho k}{\partial t} + \frac{\partial}{\partial x_i}(\rho u_i k) = \frac{\partial}{\partial x_i}\left(\left(\mu + \frac{\mu_t}{\sigma_k}\right)\frac{\partial k}{\partial x_i}\right) + S_k\,, \quad 3.9$$

$$\frac{\partial \rho \varepsilon}{\partial t} + \frac{\partial}{\partial x_i}(\rho u_i \varepsilon) = \frac{\partial}{\partial x_i}\left(\left(\mu + \frac{\mu_t}{\sigma_\varepsilon}\right)\frac{\partial \varepsilon}{\partial x_i}\right) + S_\varepsilon\,, \tag{3.10}$$

Where the source terms S_k and S_ε are defined as

$$S_k = \tau_{ij}^R \frac{\partial u_i}{\partial x_j} - \rho\varepsilon + \mu_t P_B \tag{3.11}$$

$$S_\varepsilon = C_{\varepsilon 1}\frac{\varepsilon}{k}\left(f_1 \tau_{ij}^R \frac{\partial u_i}{\partial x_j} + \mu_t C_B P_B\right) - C_{\varepsilon 2} f_2 \frac{\rho \varepsilon^2}{k} \tag{3.12}$$

Where P_B represents the turbulent generation due to buoyancy forces and can be written as: $P_B = -\frac{g_i}{\sigma_B}\frac{1}{\rho}\frac{\partial \rho}{\partial x_i}$, where g_i is the component of gravitational acceleration in the direction x_i, the constant σ_B = 0.9, and constant C_B is defined as: C_B = 1 when $P_B > 0$, and 0 otherwise;

$$f_1 = 1 + (\frac{0.05}{f_\mu})^3\,,\ f_2 = 1 - \exp(-R_T^2) \tag{3.13}$$

The constants C_μ , $C_{\varepsilon 1}$, $C_{\varepsilon 2}$, σ_k , σ_ε are defined empirically. In Solidworks Flow Simulation, the following typical values are used (SOLIDWORKS FLOW SIMULATION, 2021):

$$C_\mu = 0.09, C_{\varepsilon 1} = 1.44, C_{\varepsilon 2} = 1.92, \sigma_k = 1.3, \sigma_\varepsilon = 1$$

Where: Lewis number $Le = 1$ the diffusive heat flux is defined as:

$$q_i = \left(\frac{\mu}{Pr} + \frac{\mu_t}{\sigma_c}\right)\frac{\partial h}{\partial x_i}; i = 1,2,3. \tag{3.14}$$

Here, the constant σ_c = 0.9, Pr is the Prandtl number and h is the enthalpy. These equations describe both laminar and turbulent flows. In addition, it is possible to switch from one state to another and vice versa. Parameters k and μ_t zero for purely laminar flows.

3.1.2 Contaminant Substance:

The contaminant substance in the room diffuses in a gaseous (or liquid) form in the ambient air, called the carrier fluid. As the contaminant substance mass fraction *y* is minimal (*y<<1*), it will not impact the carrier fluid flow's properties. The contaminant substance distribution in the room is modeled using the "Tracer Study Option" of the software SolidWorks Flow Simulation. The following equation integrates the substance's non-uniform concentration and the carrier fluid's pressure gradient (SOLIDWORKS FLOW SIMULATION, 2021) (for carbonated liquids only).

$$\frac{\partial \rho y}{\partial t} + \frac{\partial}{\partial x_i}\left[\rho y u_i - \frac{\rho RT}{pm}\left(\frac{\mu}{p_r . L_e} + \frac{\mu_t}{p_{r_t} . L_{e_t}}\right)\frac{\partial y}{\partial x_i}\right] = \frac{\partial}{\partial x_i}\frac{m_1 m_2}{m^2}\left[-\frac{\rho y v_1 - y}{p}\left(\frac{\mu}{p_r . L_e} + \frac{\mu_t}{p_{r_t} . L_{e_t}}\right)\frac{\partial p}{\partial x_i}\right] \quad 3.15$$

Here, ρ is the density of both carrier fluid and substance's mixture (as $y << 1$, ρ can be considered similar for both), t is time, x_i is the $i\text{-}th$ component of the coordinate system used, u_i is the $i\text{-}th$ component of the velocity of the carrier fluid, p is the static pressure of the carrier fluid, R is the universal constant of gas. In addition, m is the molar mass (for both the carrier fluid and the substance's mixture), m_1 is the substance's molar mass, m_2 is the molar mass of the carrier fluid, v_1 is the specific volume of the substance. The other values are μ is the laminar viscosity, μ_t is the turbulent viscosity, Pr, Pr_t - the laminar and turbulent Prandtl numbers, Le, $\mathrm{Le_t}$ - the laminar and turbulent Lewis numbers, all of the carrier fluid.

3.1.3 Removal effectiveness

3.1.3.1 Pollutant (Contaminant) Removal Efficiency (CRE)

CRE measures how well the ventilation system works to clear a room of contaminants. It is defined, when more than one fluid is present in the control space, as :

$$CRE = \frac{C_e}{< C >} \quad 3.16$$

Here, C_e is the average contaminant's mass fraction flowing outside the computational domain, and $< C >$ is the average contaminant's mass fraction inside the computational domain.

A value of $CRE = 1$ means an equilibrium, an uniformly mixed system. CRE values greater than 1 mean that contaminant is removed from space, while a value less than 1 refers to an increasing contaminant concentration.

3.1.3.2 The local air quality index (LAQI):

The LAQI indicates the efficiency of the ventilation system in removing polluted air from a specific point in the computational domain. It can be defined when there is more than one fluid in the control space as :

$$LAQI = \frac{C_e}{C} \quad 3.17$$

Where C_e is the average contaminant's mass fraction flowing outside the computational domain and C is the mass fraction of the contaminant at a specific point. A value of *LAQI = 1* characterizes a perfectly mixed system. Otherwise, a higher *LAQI* value at a point characterizes a greater capability of the ventilation system to exhaust polluted air from that point.

3.1.4 Thermal Comfort

These criteria are used when designing occupied spaces and their HVAC systems to determine whether the environmental conditions are acceptable in general thermal comfort and air quality or represent discomfort. The fluid flow (which is the air) is calculated to detect the comfort parameters by thermal sensation and degree of discomfort (thermal

dissatisfaction) for people exposed to moderate thermal environments (SOLIDWORKS FLOW SIMULATION, 2021), in this research two of these criteria are chosen.

3.1.4.1 Predicted Mean Vote (PMV)

PMV is an indicator that predicts the average voice value of a large group of people on a 7-point thermosensitive scale (-3 to +3) where -3 indicates cold, +3 indicates heat, and 0 represents normal temperature, according to the human body. Thermal equilibrium is reached when the body's internal heat production equals the heat loss to the environment. Therefore, in a temperate environment, the human thermoregulation system will automatically attempt to adjust the skin temperature and sweat secretion to maintain thermal balance (*ASHRAE STANDARD*, 2010), PMV is defined as follows:

$$\begin{aligned} PMV = (0.303e^{-0.036M} + 0.028).\{(M-W) - 3.0 \\ \cdot 10^{-3}[5733 - 6.99(M-W) - P_a] - 0.42[(M-W) - 58.15] \\ - 1.7 \cdot 10^{-5} M(5867 - P_a) - 0.0014M(34 - T_a) - 3.96 \\ \cdot 10^{-8} f_{cl}[(T_{cl}+273)^4 - (T_r+273)^4] - f_{cl}h_c(T_{cl} - T_a)\} \end{aligned} \quad 3.18$$

$$\text{Here: } T_{cl} = 35.7 - 0.028(M-W) - I_{cl}\{3.96 \cdot 10^{-8} f_{cl}[(T_{cl}+273)^4 - (T_r+273)^4] + f_{cl}h_c(T_{cl} - T_a)\} \quad 3.19$$

$$h_c = max\{2.38(T_{cl} - T_a)^{0.25}, 12.1\sqrt{V}\} \quad 3.20$$

$$f_{cl} = \begin{cases} 1.00 + 1.29I_{cl}, for\ I_{cl} \le 0.078 \dfrac{m^2}{kW} \\ 1.00 + 0.645I_{cl}, for\ I_{cl} > 0.078 \dfrac{m^2}{kW} \end{cases} \quad 3.21$$

Here: M is the metabolic rate (W/m^2 of body surface) is the conversion rate of chemical energy into heat and mechanical work by metabolic activities within an organism (it is set by default at 70 W/m^2), W is the external work ($W/m^2$of body surface), which represents the effective mechanical force (the default value is 0 W/m^2), I_{cl} is the clothes the thermal resistance (W/m^2). The clothing set provides a reasonable resistance to heat

transfer. The definition of clothing insulation relates to heat transfer from the whole body and, therefore, includes exposed parts of the body, such as the head and hands. Typical thermal resistance values for a particular clothing group by default it is set to (0.11 m^2 K/s), f_{cl} is the ratio of the dressed surface to the bare surface, T_a is the air temperature (K), T_r is the mean radiant temperature (K), V is the relative air velocity (m/s), P_a is the partial pressure of water vapor, (P_a) calculated according to the saturation curve, the air temperature T_a and the relative humidity, h_c is the convective heat transfer coefficient (W/m^2/K), T_{cl} is the surface temperature of the garment (K).

3.1.4.2 The predicted percentage of dissatisfaction (PPD)

PPD is defined as a determinant that provides information on thermal dissatisfaction by predicting the percentage of people likely to be too hot or too cold in a given environment (*ASHRAE STANDARD*, 2010). It can be obtained using the following equation:

$$PPD = 100 - 95EXP(-0.03353PMV^4 - 0.2179PMV^2) \quad 3.22$$

3.2 GEOMETRY (DOMAIN CONTROL)

During the present research, a prototype for a hospital isolation room was developed. Three models have been added inside the room, the bed being the first one. The other two models represent the health care worker (HCW) standing beside the bed and the patient lying on the bed. The air in the room is conditioned and refreshed by the inlet, while exhaled air is released through the outlet. Three light bulbs are mounted overhead, as shown in Figure 1. Previous studies suggested some designs that achieved optimum performance by either removing contaminants or enhancing thermal comfort. Owing to that, an investigation was done to illustrate how these designs influence the environment inside the space. Each design has three different airflows 9, 12, and 15 ACH, respectively. In cases 1,2, and 3 the place of the air inlet with a distance from the ceiling of 0.5 m, and the outlet is 1 m from the floor as

shown in Figure 2. Figure 3 demonstrates cases 4,5, and 6 the place of the inlet with a distance from the ceiling of 0.5 m, and the outlet is 0.5 m from the floor. The first two designs are recommended by Çuhadaroğlu & Sungurlu (2015). In cases 7, 8, and 9 the inlet is behind HCW, and the outlet exists in front of the HCW with a distance of 0.5 m from the floor and the roof as shown in Figure 4, this design is selected by Thatiparti *et al* (2017). Figure 5 shows cases 10, 11, and 12 chosen by Cho (2019), where the inlet and outlet are located on the roof the inlet is far 1 m from the side wall and the outlet is positioned from the other side wall with 0.5 m Table 2 have a summary of these designs. The dimension of the room, the inlet, and the outlet are mentioned in Table 1.

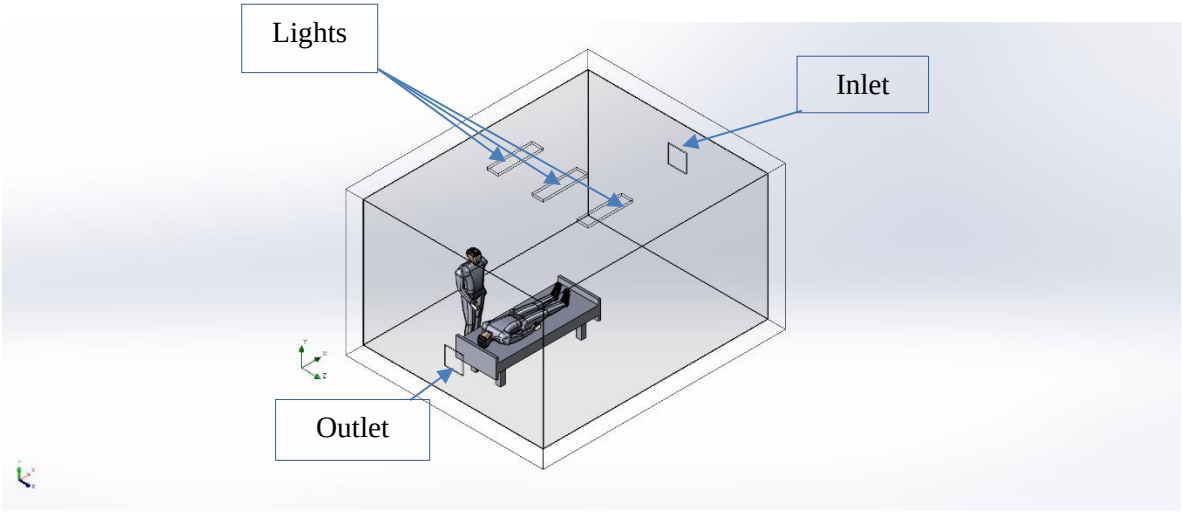

Figure 1 : Isolation Room and It's Content

Table 1 Dimensions Details of The Domain

	Length (m)	**Width (m)**	**Height (m)**
Room	5.00	4.00	2.8
Diffusers	0.4	0.4	
Bed	2.2	0.9	0.4
Manikin	1.75	0.6	

Table 2 Cases Number and Location of Air Diffusers for Each Case.

Case no.	**Air Inlet**	**Air Outlet**	**Distance** (m)	**Ventilation Volume** (m^3/s)
01	Sidewall	Sidewall	AI=0.5 roof, AO=1 floor	0.14
02	Sidewall	Sidewall	AI=0.5 roof, AO=1 floor	0.18
03	Sidewall	Sidewall	AI=0.5 roof, AO=1 floor	0.23
04	Sidewall	Sidewall	AI=0.5 roof, AO=0.5 floor	0.14
05	Sidewall	Sidewall	AI=0.5 roof, AO=0.5 floor	0.18
06	Sidewall	Sidewall	AI=0.5 roof, AO=0.5 floor	0.23
07	Behind the HCW	Infront of HCW	AI= AO=0.5 roof & floor	0.14
08	Behind the HCW	Infront of HCW	AI= AO=0.5 roof & floor	0.18
09	Behind the HCW	Infront of HCW	AI= AO=0.5 roof & floor	0.23
10	Roof	Roof	AI=1 SW AO=0.5 SW	0.14
11	Roof	Roof	AI=1 SW AO=0.5 SW	0.18
12	Roof	Roof	AI =1 SW AO=0.5 SW	0.23

AI: Air Inlet, AO: Air Outlet, SW: Side Wall.

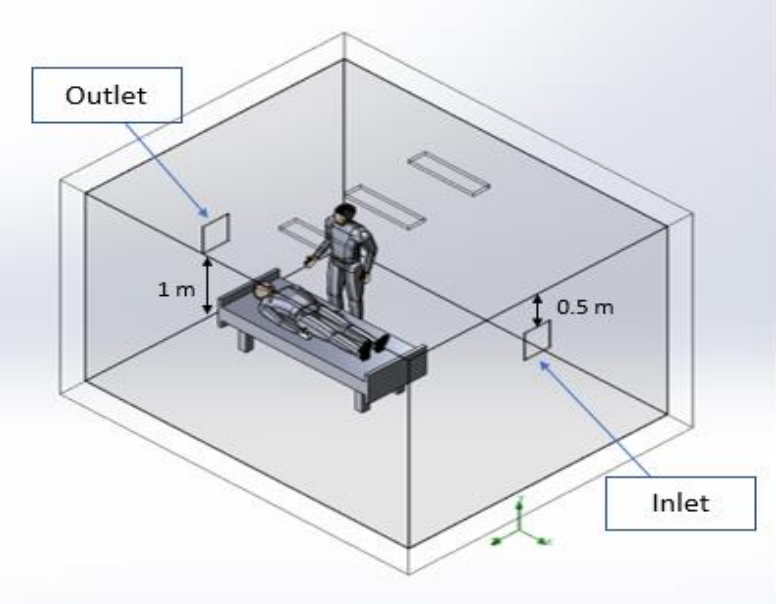

Figure 2 : Geometry for Cases 1, 2, and 3

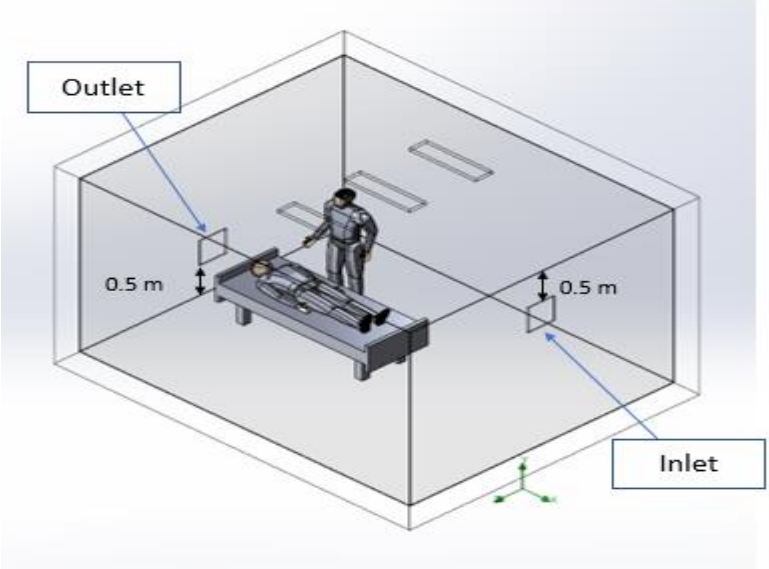

Figure 3 : Geometry for Cases 4, 5, and 6

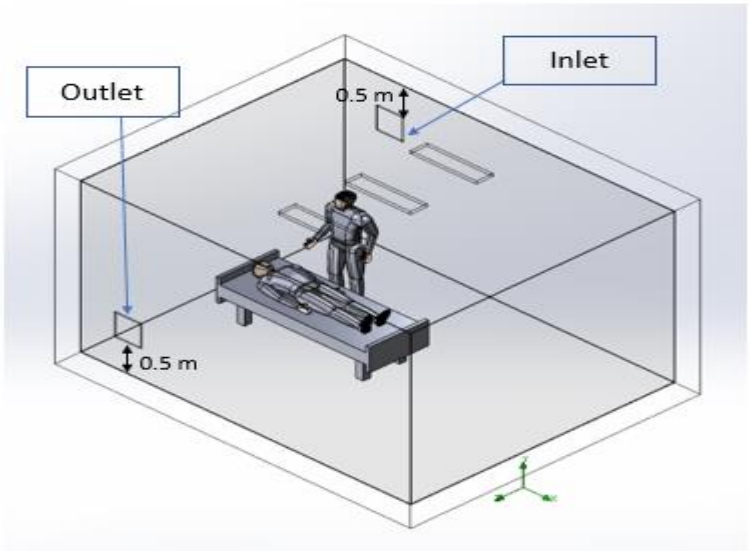

Figure 4 : Geometry for Cases7, 8, and 9

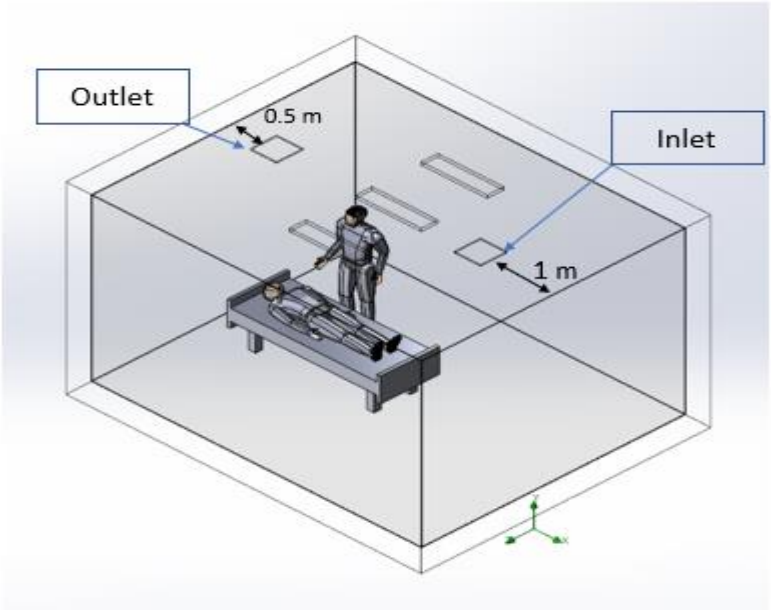

Figure 5 : Geometry for Cases 10, 11, and 12

3.3 BOUNDARY CONDITIONS

Since boundary conditions are of primary significance in attaining desirable outcomes, it was essential to define them precisely. Hence, HVAC standards were reviewed, and a literature survey was done. Steady-state simulations are performed to verify pollutant concentration and thermal comfort through different ventilation designs. Initially, the airflow supply was maintained at 9 ACH with no return air (Lu *et al*., 2020). Afterward, the 12 and 15 ACH were applied. For the system airborne infectious isolation rooms (AIIR), according to the American standard ASHRAE 170 (*Ventilation of Health Care Facilities*, 2020), the pressure difference is essential to be maintained, and it was set $at\ 2.5\ Pa$ at the outlet. Heat sources for both the health care worker and patient, as well as the ceiling light, have been chosen to be $144\ \mathrm{W/m^2}$, $81\ \mathrm{W/m^2}$, and $11\ \mathrm{W/m^2}$, respectively (Ahmed, 2012), (*Ventilation of Health Care Facilities*, 2020). In addition, it was assumed that the walls are adiabatic, with no heat transfer or storage within, and the air inlet temperature is $298\ K$ while the initial room temperature is $289\ K$ the pressure is $101{,}325\ Pa$ and the relative humidity is 50%. Moreover, pollutants are represented by carbon dioxide, exhaled through the patient's mouth with a mass flow of $0.00014\ kg/s$, at a temperature of $307\ K$with 100 % humidity (Yoon *et al*., 2016), (Lu *et al*., 2020). The turbulence intensity in the inlet was set at 20% within the recommended limits (10-30%) (Cehlin & Moshfegh, 2010). For the low-velocity value, 2% has been chosen in the range of 1-5% (Cao *et al*., 2011). The length scale variation does not influence the flow pattern at a low inlet turbulence intensity value. However, its effect starts to appear from the 40 % value of turbulence intensity. Based on the perimeter, the turbulence length was chosen for both the inlet and the patient's mouth (Gao & Niu, 2006). Table 3 indicates the majority of these boundaries.

Table 3 Defined Boundaries

	Type	Value
Room Air	Temperature Initial	289 K
	Pressure	101,325 Pa
	Humidity	50%
	Turbulence Tensity	2%
	Turbulence Length	0.335 m
Supply Air	Volume Flow	0.18 $m3/s$
	Temperature	298 K
	Pressure	101,325 Pa
	Humidity	50%
	Turbulence Tensity	20%
	Turbulence Length	0.16 m
Air Expired	Mass Flow	0.00014 kg/s
	Temperature Initial	307 K
	Pressure	101,325 Pa
	Humidity	100%
	Turbulence Tensity	2%
	Turbulence Length	*0.12 m*
Exhaust	Pressure	101,322.5 Pa

3.4 MESH SETTING

SolidWorks software was used in this study to create a tetrahedral-structured grid to capture the behavior of the thermal environment and the CO_2 particles. The domain has been split through a computational mesh to the cartesian global coordinate system's axes to form rectangular parallelepipeds called cells with a set of orthogonal planes. First, the original parallelepiped cells containing boundaries are split into several parts. The basic mesh is a mesh of coarse levels cells, which is constructed for the whole domain at the beginning of the process and formed by dividing the domain by parallel planes into slices orthogonal to the Global Coordinate System's axes. Next, the local mesh is refined by splitting a rectangular computational mesh cell into eight cells through three orthogonal planes that divide the cell's edges into halves. In this study, two types of mesh were included. Firstly, the refinement mesh (local mesh) was done on the area around the occupants, the diffusers, and the lamps at high temperatures. At the same time, the coarse grids were selected for the remaining area.

The following input parameters (SOLIDWORKS FLOW SIMULATION, 2021):

i. Problem type (Internal\External, Compressible\Incompressible, 3D\2D)

ii. Minimum gap size (h_{gap}) and minimum wall thickness (h_{wall})

iii. Level of initial mesh (L_{ini})

iv. Computational model bounding box (B_{model})

v. Fluid region bounding box (B_{fluid})

vi. Symmetry settings applied to the computational domain boundaries

vii. Middle size of the computational model (H_{mean})

viii. Wind direction for external flows (e_{wind})

The Level of the initial mesh (L_{ini}) is specified between (3-7) for each mesh, respectively, and the minimum gap size (h_{gap}) is selected as $0.01\ m$. This ensures that the flow passage through the gap is larger than the specified minimum gap size. The local mesh was chosen to get results with more accuracy. Local settings help solve a specific area within a complex model, which is sensitive to the base grid. The local mesh was applied as a cube surrounding the occupants (the area of interest). Refining fluid cell level and the fluid/solid boundary are chosen with a value of 1. More than this value, there was no stability in the results, although the study is steady state. The minimum wall thickness (h_{wall}) was determinate $(0.01)\ m$, where the value of y^+ near the wall is equal to 10 (Mousavi, 2015).

3.4.1 Mesh Convergence Study

Different numbers of grids have been used in this study. Five simulations were carried out from 125,843 to 3,680,531 cells to increase the precision of the results as demonstrated in (Figure 6 until Figure 10). Figure 11 is revealed a side view of the finest grid. In addition, Figure 12 and Figure 13 are shown the difference in the level of the grid for the patient and the inlet, respectively. In order to reveal the convergence a point of interest was chosen in the domain to test the changes in temperature throughout the refined meshes. Figure 14 illustrates the error in temperature value according to the number of elements. The convergence error is reduced to 0.16%. According to Hallé (2016), a convergence error of less than 5% is acceptable. This accuracy is enough for doing the simulations, considering the power of the CPU, the domain magnitude, and the complicated curvy surfaces (Georges, 2017).

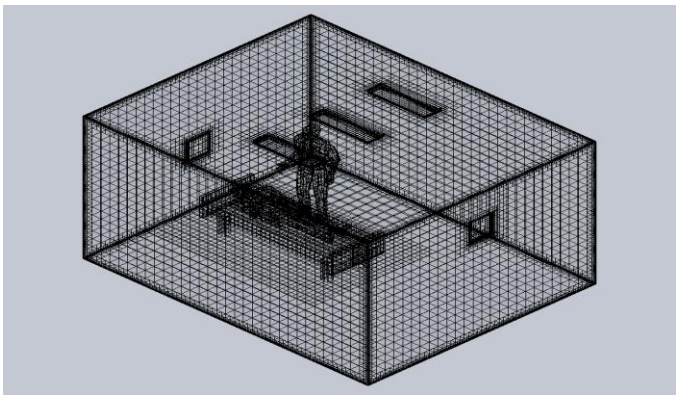

Figure 6 : Surface Plot 125,843 Cells

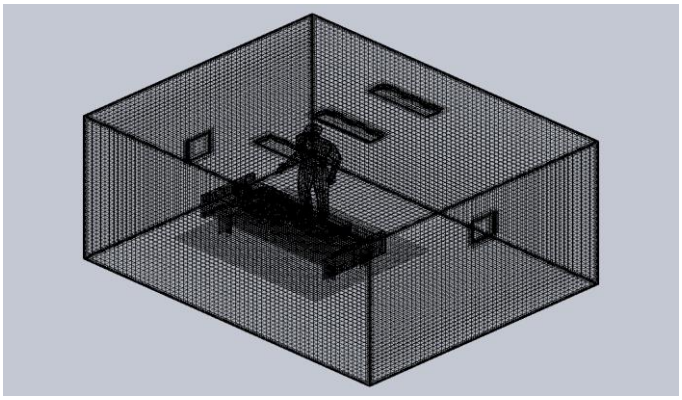

Figure 7 : Surface Plot 820521 Cells

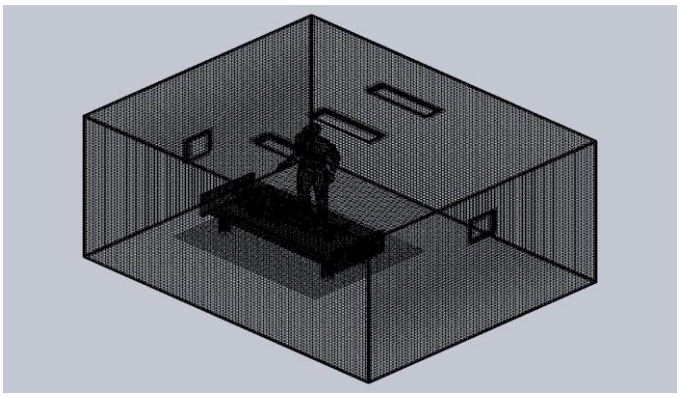

Figure 8 : Surface Plot 1508968 Cells

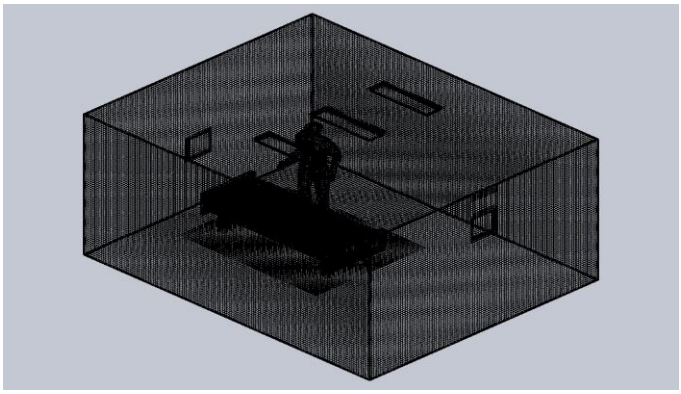

Figure 9 : Surface Plot 2460313 Cells

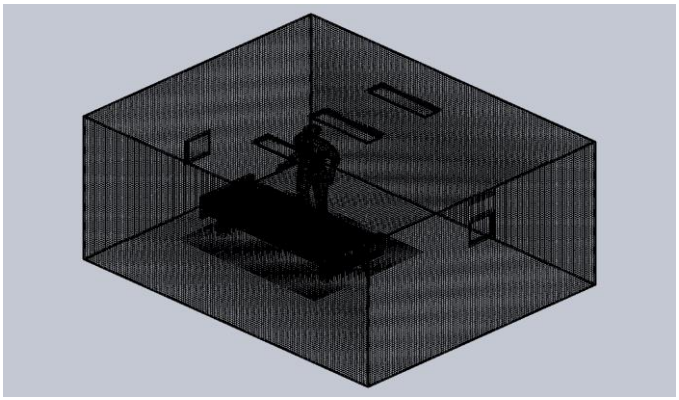

Figure 10 : Surface Plot 3680531 Cells

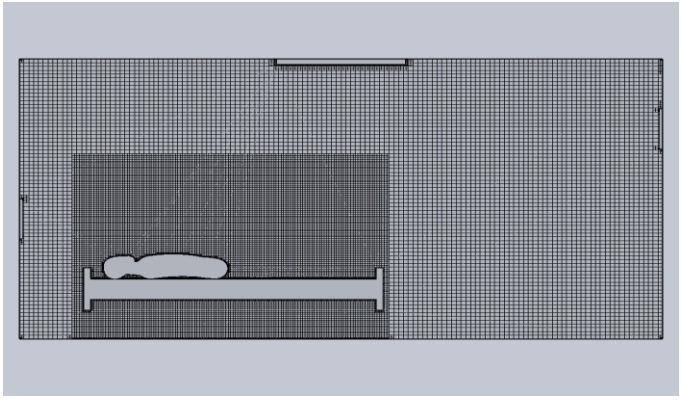

Figure 11 : Cut Plot 3680531 Cells

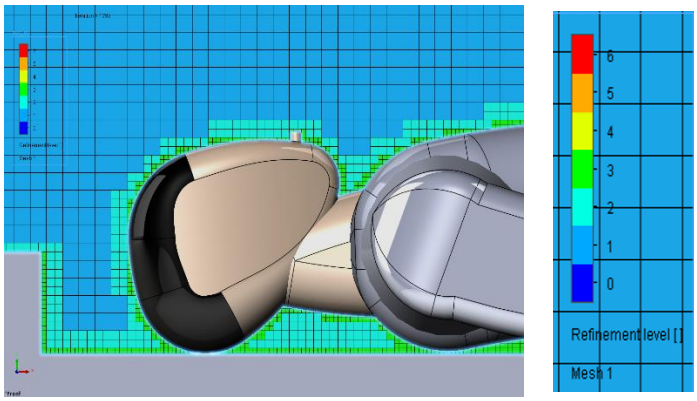

Figure 12 : Cut Plot Refinement Level Close to The Patient at 3680531 Cells

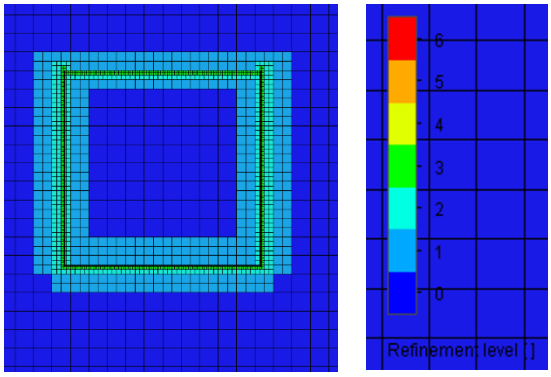

Figure 13 : Cut Plot Refinement Level Close to The Vent Opening at 3680531 Cells

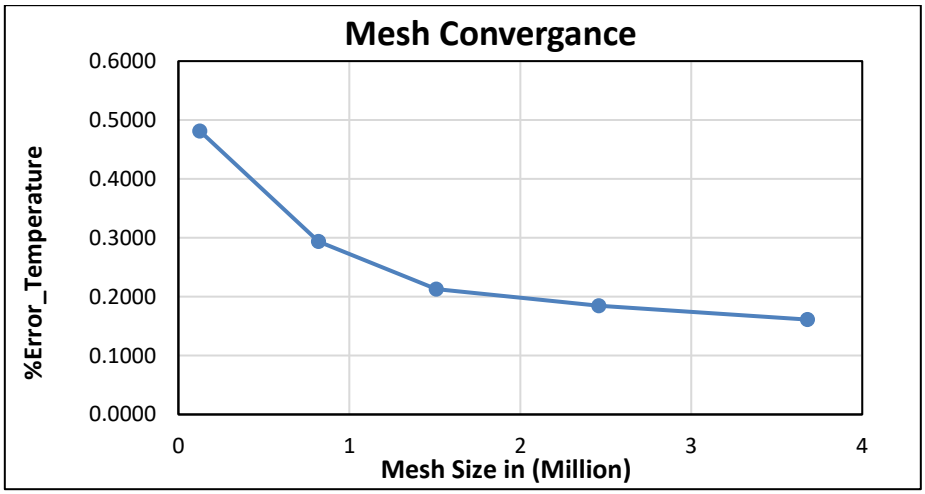

Figure 14 : Mesh Independence (%Error_Temperature) vs. Number of Elements.

3.5 SOLUTION CONVERGENCE CRITERIA

When the residual for mass conservation stabilizes, converged solutions are retrieved for all situations. Convergence occurs when the solution no longer changes with successive iterations (Mekbib Kifle, 2018). The convergence is obtained with around 1100 iterations with a solution time was around 28 hours for each case. As shown in Figure 15, where these iterations are incorporated within each time step and repeated until a solver convergence is attained (SOLIDWORKS FLOW SIMULATION, 2021). The computer was used with a processor i9-9900K CPU and 64Gb RAM with full capacity.

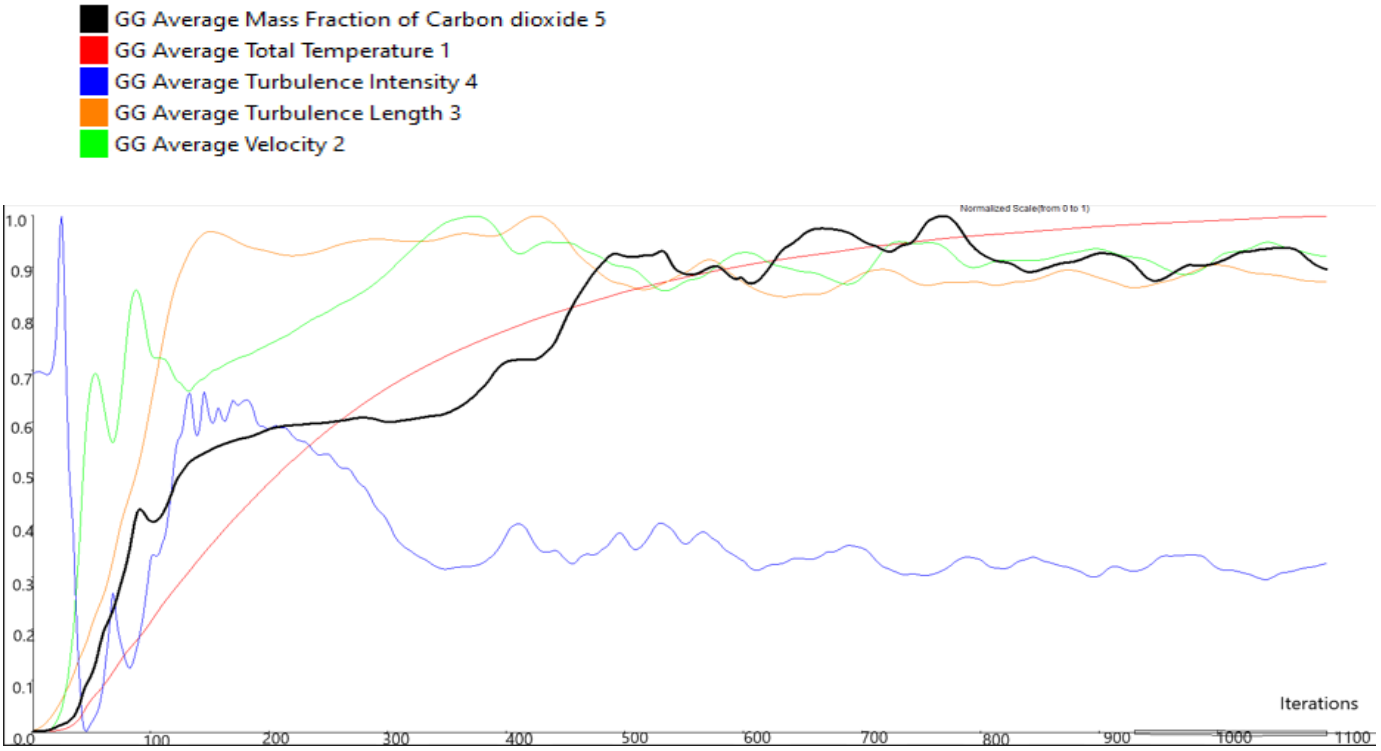

Figure 15 : Residuals for Conserved Variables for Case 3 at 15 ACH

3.6 VALIDATION OF THE NUMERICAL SOLUTION

A validation study was performed with the experimental readings of temperature with a similar study that has an experimental side done by Berlanga *et al*. (2018). This study has an isolation room was established with the same airflow rate of 12 ACH, and similar locations for the inlet and the outlet. Figure 16 shows a vertical line next to the patient where the temperature values are taken. The CFD simulations furnished a good accuracy in values of temperature as (Figure 17) illustrates that there is proximity is achieved between the values with an error percentage of 1.09%.

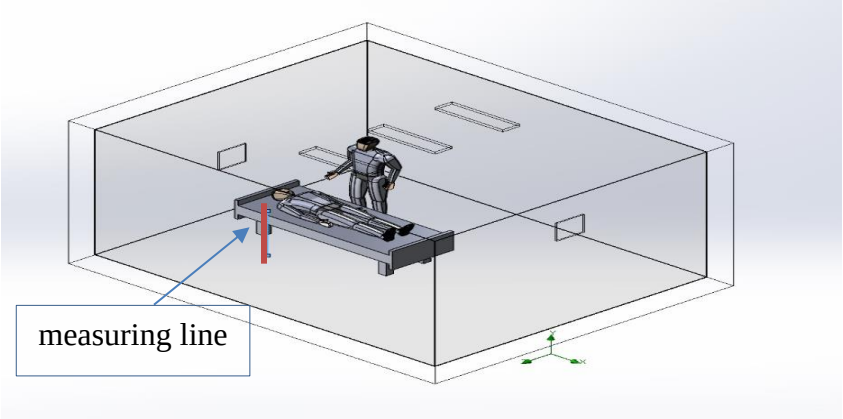

Figure 16 : Illustration of The Position of the Measuring Line

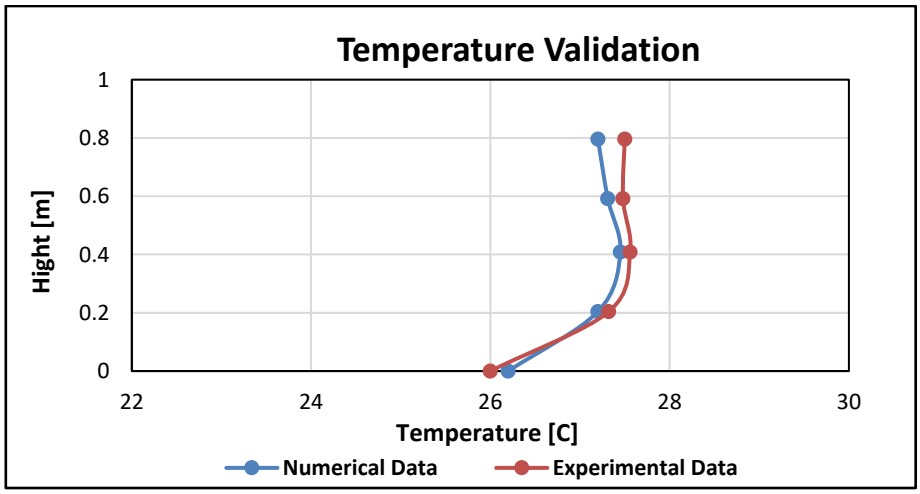

Figure 17 : The Comparison with an Experimental Study

CHAPTER 4 RESULTS

The purpose of this chapter is to display the ventilation scenarios by presenting the outcomes of the simulation studies for the various strategies for adjusting the flow and the location of the air diffusers. The results allow us to understand how thermal comfort and the mechanism of pollution transmission would be affected by these adjustments and to find the optimum case through the results. The results will include; PPD and PMV to indicate thermal comfort, LAQI of CO_2, and a tracing study of CO_2 (flow trajectories) for describing the altitude of pollutants. The results will be interpreted using the front view, top view, and surface shape for flow trajectories. Charts will display the results, which depend on a line drawn at a vertical distance of 1 m from the ground and is parallel to the patient through a distance of 2 m, as shown in Figure 18. The different simulation cases are described in Table 2.

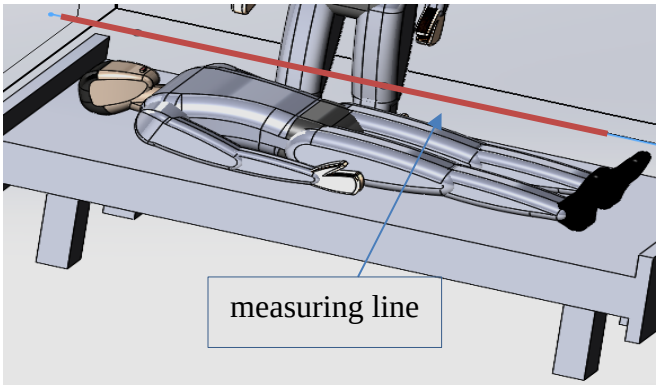

Figure 18 : Illustration of the position of the Line Probe

4.1 RESULTS OF CASES 1, 2, AND 3

As mentioned previously each design has three cases with each case having different airflow. In this design, the inlet is close to the ceiling at 0.5 m, and the outlet is located on the other side behind the patient at level 1 m from the floor as shown in Figure 2.

4.1.1 Predicted Mean Vote (PMV)

The thermal balance between the human body and the surrounding environment can be seen in Figure 19 at 9 ACH. The majority of the area in yellow in Figure 19 (a) is about 1.29 PMV, indicating a warm atmosphere inside the space. The airflow direction path is shown in green at about 0 PMV, which refers to a feeling of thermal comfort, except for the upper region, represented in red, where the value is 3 PMV. The temperature is higher due to the hot air's buoyancy and the lights' thermal load. In the case of 12 ACH (Figure 19 (b)), there is an indication that the green area has been expanded due to increased air volume supplied as per equation 3.18. The airflow has a significant role in PMV, as shown at 15 ACH (Figure 19 (c)), where most of the region is green; 0 PMV. The presence of a green area indicates neutral feelings, which is up to the upper level, except for some regions around the occupied area that are yellow and red near the patient. Due to the flow becoming horizontal, air will not pass through the occupied area, which leads to the accumulation of heat in the occupied area.

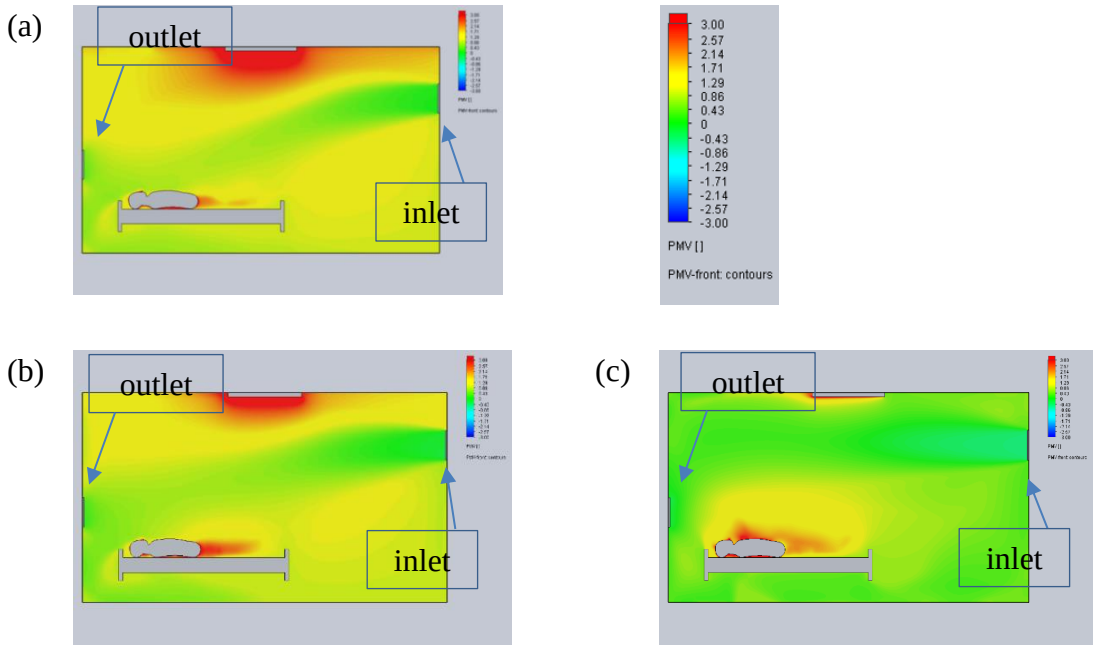

Figure 19 : Front View of PMV (a) Case 1 at 9 ACH (b) Case 2 at 12 ACH (c) Case 3 at 15 ACH

4.1.2 Predicted Percent Dissatisfied (PPD)

Thermal dissatisfaction is another way to express thermal comfort by taking a group of people's opinions shown as a percentage. The ideal value is 0 for the PPD, indicating that everyone is comfortable with the environment's temperature. For example, in Figure 20 (a & b), approximately 25% of PPD in the unoccupied regions are not satisfied with the temperature of the space except for the patient's area, which has a positive effect owing to the passage of the air path and its descent down to the level of the occupied region due to gravity and the low speed of air. In contrast, for 15 ACH (Figure 20 (c)), the value is between 0-7%, which corresponds to the value suggested by Karimipanah *et al*. (2012), which should not exceed 10%. However, the occupied area still has a high value of PPD due to the airflow direction. This indicates that a rise in airflow positively affects thermal comfort if it is

appropriately diffused. Figure 21 clarifies the variance between the value of PPD above the patient at the height of 1 m. It could be noticed that cases 1 and 2 have close values of PPD and there is an alternation of values. while case 3 was the worse, where the value of PPD reach 40%.

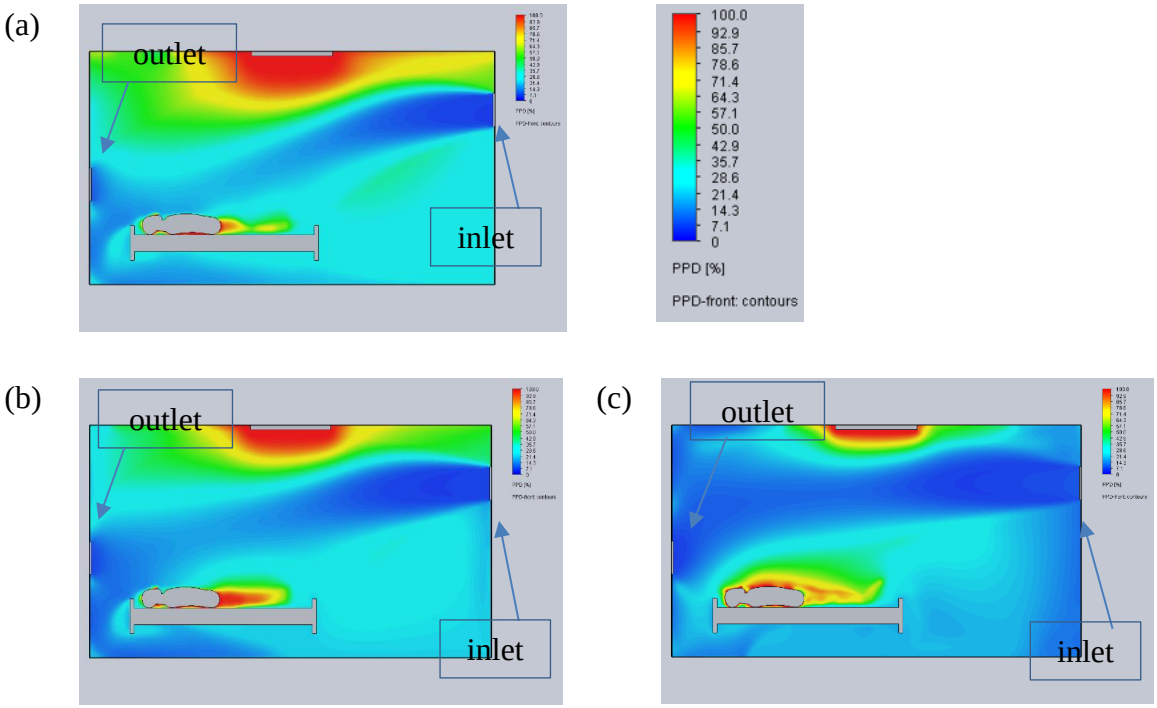

Figure 20 : Front View of PPD (a) Case 1 at 9 ACH, (b) Case 2 at 12 ACH (c) Case 3 at 15 ACH

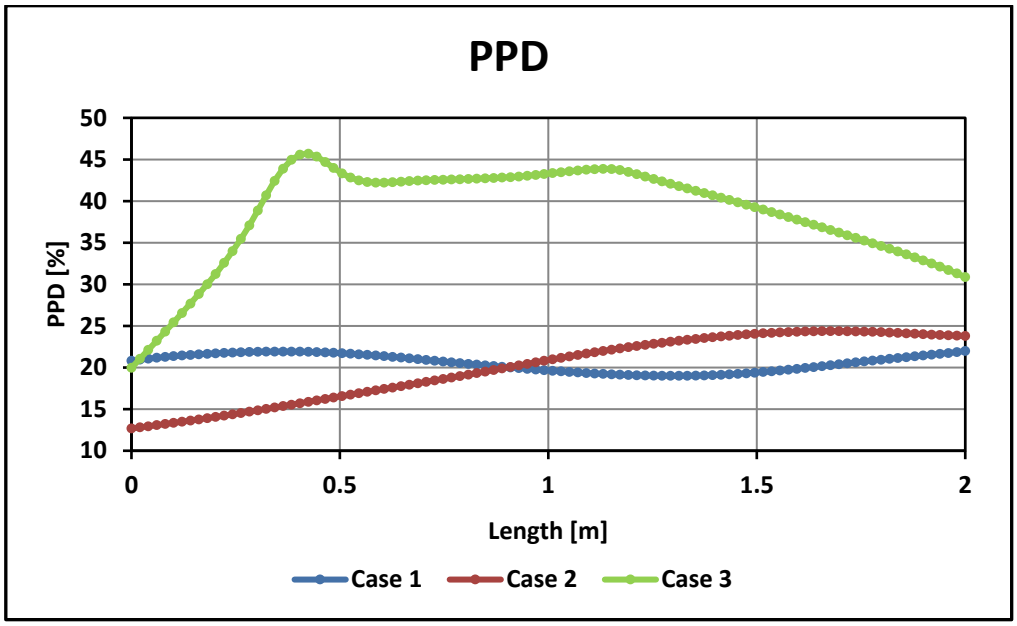

Figure 21 : Chart Shows the PPD % at Line Probe

4.1.3 Local Air Quality Index (LAQI)

Using carbon dioxide as a proxy for the exhaled contaminant is one of the ways to study the air quality. Results levels were taken at the height of 1 m from the ground. Pollutant concentrations are lower when the value of LAQI is high. Figure 22 (a) indicates that the area near the exhaust is the best one for removing pollutants. Especially at the center of the outlet, pollutants gradually decrease away from the outlet. In contrast, the HCW area behind the bed and the area near the inlet is less effective in removing contaminants as the force of the air is not strong enough to push the pollutants toward the outlet. At 12 ACH (Figure 22 (b)), it can be observed that the effectiveness decreases at the lower part of the outlet level, while it is higher in the upper part, up to the inlet level. The effectiveness in the upper part will be revealed in the Trace Study of CO2 (Flow Trajectories) section of each case. When the amount of ventilation is increased to 15 ACH (Figure 22 (c)), is found that an increase in the amount of air reduces the pollutant's concentration. This result agrees with the findings of Ameer *et al*. (2021), as they found that a higher airflow velocity results in a larger polluted

region but with a lower concentration of pollutants as the particles are forced out of the outlet more quickly.

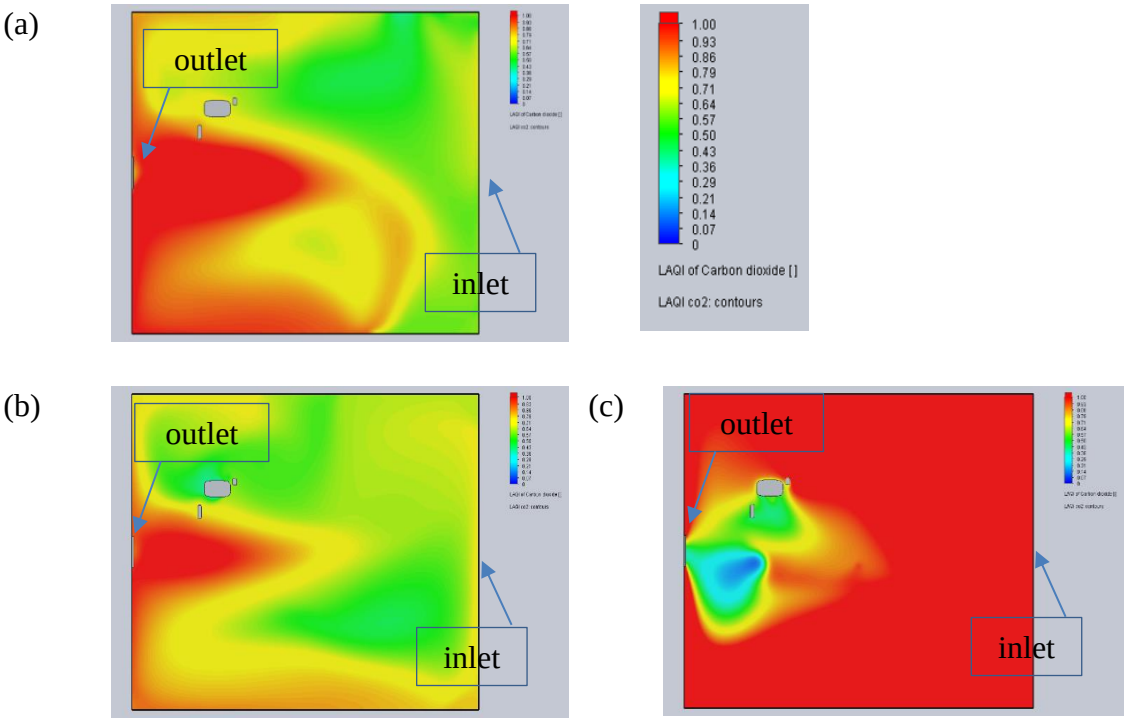

Figure 22 : Top View of LAQI of CO_2 (a) Case 1 at 9 ACH (b) Case 2 at 12 ACH (c) Case 3 at 15 ACH

4.1.4 Trace Study of CO_2 (Flow Trajectories)

As mentioned, the pollutants will be represented by the carbon dioxide emitted by the patient's exhale, with its movement and concentration all over the room. The concentration is given with particles per million ppm. The flow from the patient's mouth has been considered 0.00014 kg/s. At a level of 1 m, it is noticed there is less concentration at the outlet and minor concentrations inside the air stream at 9 ACH (Figure 23 (a)). However, at 12 ACH (Figure 23 (b)), it is found that the mixing is more significant, and the pollutant

concentration is lower on the opposite side of HCW. However, the area of HCW still has a high pollution concentration. On the contrary, at 15 ACH (Figure 23 (c)) demonstrates that a larger air volume is better for pollutant removal, while some contaminants are still contained under the inlet.

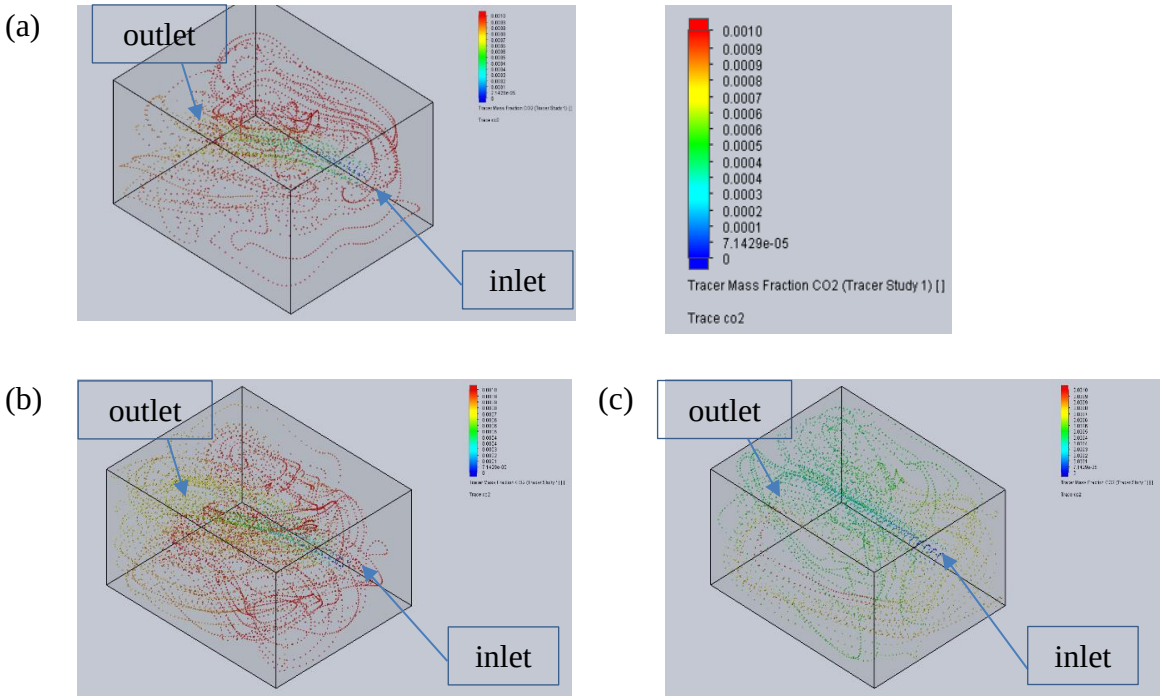

Figure 23 : Flow Trajectories of Trace Study of CO_2 (a) Case 1 at 9 ACH (b) Case 2 at 12 ACH (c) Case 3 at 15 ACH

4.1.5 Turbulence Intensity

In the boundary conditions of the $k-\varepsilon$ turbulence model, the turbulence intensity, I, is defined as the root-mean-square of the velocity variations divided by the mean flow velocity. Low turbulence is typically defined as an intensity of 1% or less, According to the cited international norms, the typical level of turbulence is lower than 30% (Basse, 2019), (Baylar *et al*., 2009), and (Ležovič *et al*., 2013). The outcomes show that the intensity value

was determined in boundary conditions but varied according to the different flows. At the patient's head close to the outlet, the values appear to be somewhat close to the chosen value; as the vortex forms beside the airflow path where the air path is curvey and the airflow reach the head area directly, which pushes the turbulence outside of the bed. The values range between 25-37% above the patient for 9 and 12 ACH in (Figure 24 (a & b)). But from 1.5 m and towards the inlet, high turbulence intensity values are noticed, especially at 15 ACH (Figure 24 (c)). The peak was found at 70%, as shown in the chart below (Figure 25).

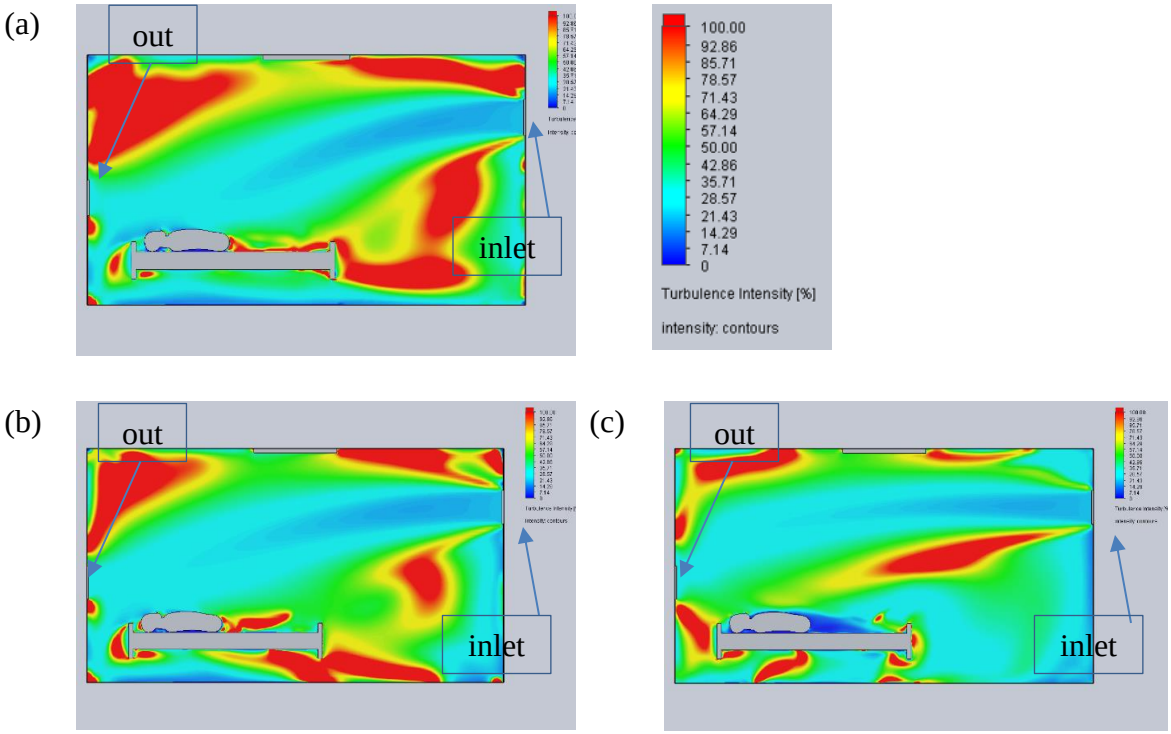

Figure 24 : Front View of Turbulence Intensity (a) Case 1 at 9 ACH (b) Case 2 at 12 ACH (c) Case 3 at 15 ACH

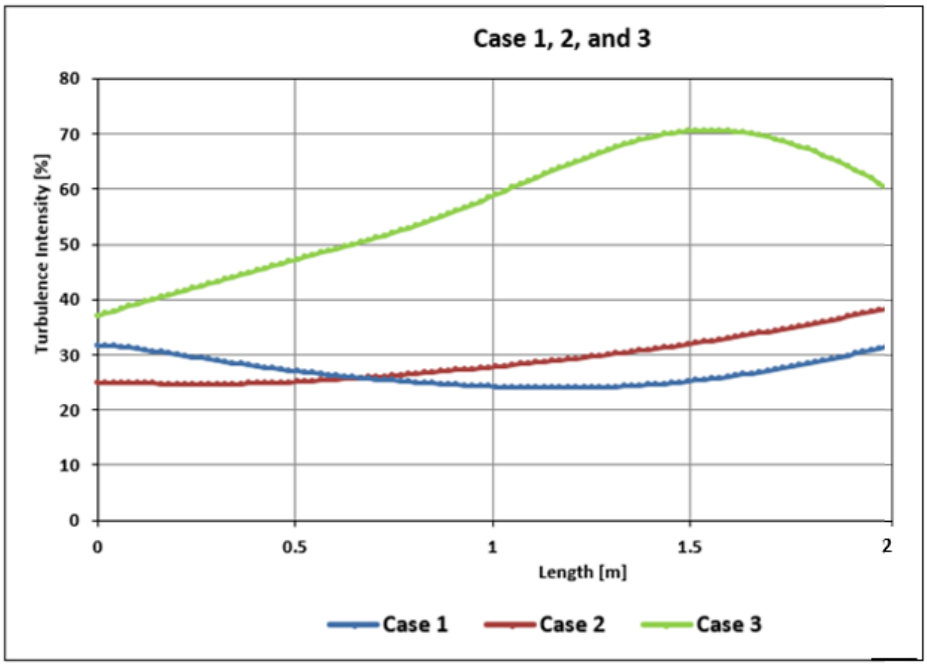

Figure 25 : Chart Shows the Turbulence Intensity at Line Probe

4.1.6 Contaminant Removal Effectiveness & Air Diffusion Performance Index (CRE) & (ADPI)

CRE values for the three different flows in case 3 achieved the optimum removal, as shown in Table 5 below. Values CRE ≥ 1 means it efficiently removes the contaminated air from the space, and below 1 has poor effectiveness. It is found that at 15 ACH case 3, is considered the best scenario for removing the pollutants, which intersects with the search results (Ameer *et al*., 2021) because of the increased airflow. ADPI represents the whole computational domain when the speed is less than 0.35 m/s, and the draft air temperature falls by values between -1.5 and $\pm 1\,K$. The results of ADPI revealed how much the percentage of air diffusion in each case was achieved. Case 3 was the optimum one, as the value is more than 80% according to Rusly *et al*. (2014).

Table 4
CRE & APDI Values for Cases 1, 2, and 3

	9 ACH	12 ACH	15 ACH
CRE	0.70	0.65	1.15
APDI %	72.8	77.4	85.4

4.2 RESULTS OF CASES 4, 5, AND 6

In the following cases, the design is similar to the previous one with a difference in outlet location. The new position is fam 0.5 m from the floor instead of 1 m as shown in Figure 3.

4.2.1 Predicted Mean Vote (PMV)

Similar results were found for cases 4, 5, and 6 compared to cases 1, 2, and 3. For 9 ACH (Figure 26 (a)), as can be seen, the green area is concentrated above the occupied region because the airflow path reaches up to the patient's line. In addition, the outlet absorbs the air directly, which doesn't allow the air to move around the room, leading to thermal discomfort for a large part of the room. While at 12 ACH (Figure 26 (b)), a green area increases significantly throughout the room, owing to the increase in the airflow. Moreover, the value of PMV gradually rises in the patient’s area, which means a more uncomfortable feeling because the supplied air tends to become parallel to the patient. The upper area has good thermal comfort values for 15 ACH (Figure 26 (c)). However, the bed area has an undesirable value of PMV because the airflow is more substantial and thus becomes almost entirely horizontal.

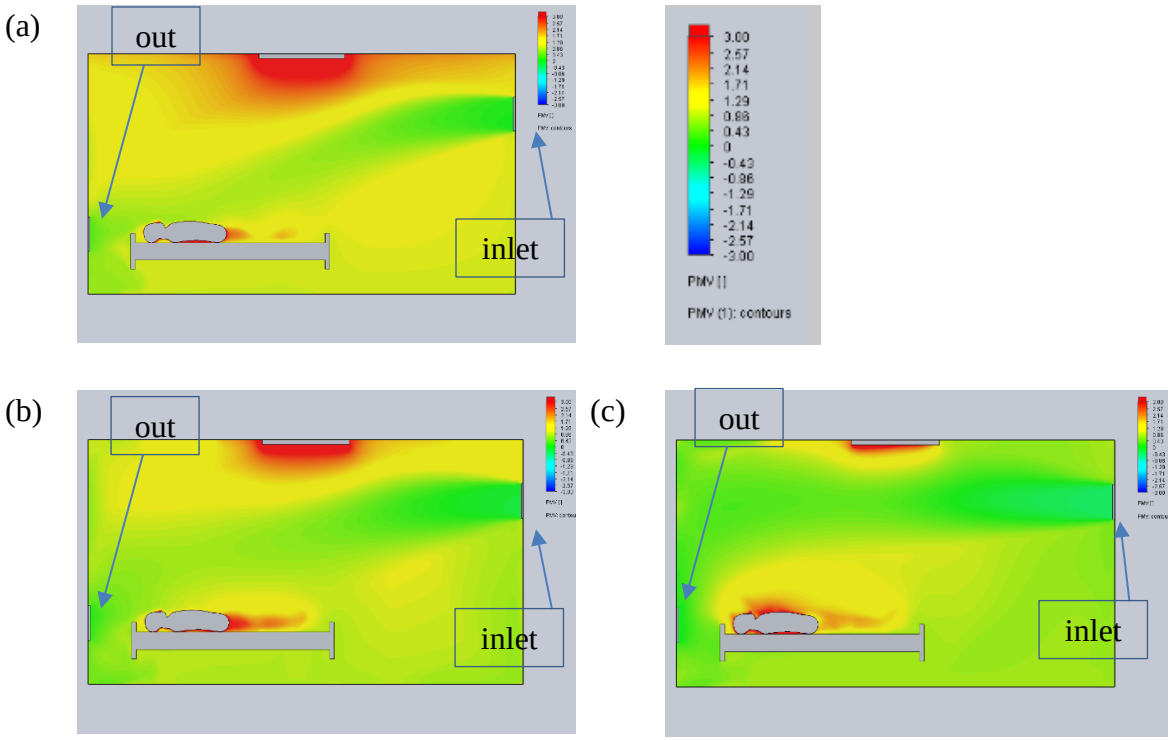

Figure 26 : Front view for PMV (a) Case 4 at 9 ACH (b) Case 5 at 12 ACH (c) Case 6 at 15 ACH

4.2.2 Predicted Percent Dissatisfied (PPD)

It has been observed that by repositioning the outlet, the outcomes are similar to the results in cases 1, 2, and 3 according to the thermal simulation results. In this design (Figure 3), for 9 ACH (Figure 27 (a)), the only variance is the level of thermal satisfaction, which decreases near the ground due to the location of the outlet. While at 12 ACH (Figure 27 (b)), it is noticed that there was a more practical consequence on the expansion of the thermal satisfaction area. Throwing the air with more force causes the air path to becoming horizontal instead of going downwards because of gravity, which assists in making more exchange. At 15 ACH (Figure 27 (c)), there was a correspondence with case 3 (Figure 19 (c)) due to the strength of the flow. Moreover, there is no significant effect on the outlet's location between

these two designs (Figure 2 and Figure 3). However, comparing the charts in Figure 28 and Figure 21, cases 1, 2, and 3 have better results.

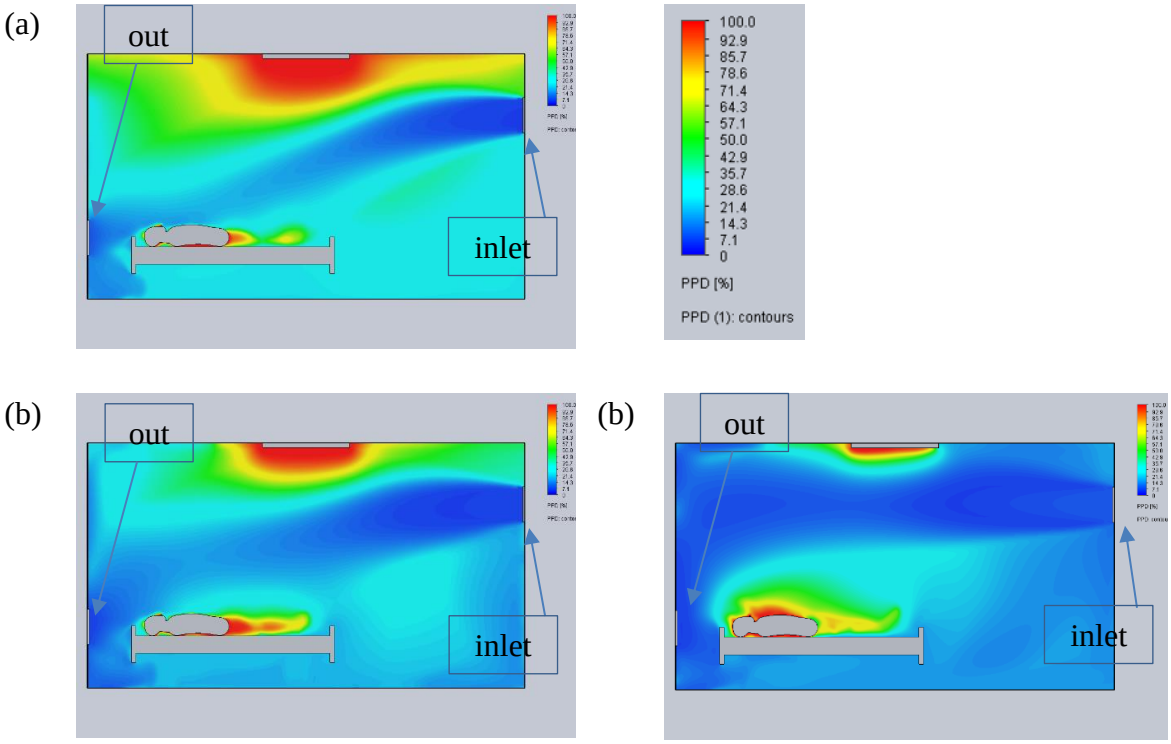

Figure 27 : Front view for Fluid PPD (a) Case 4 at 9 ACH (b) Case 5 at 12 ACH, (c) Case 6 at 15 ACH

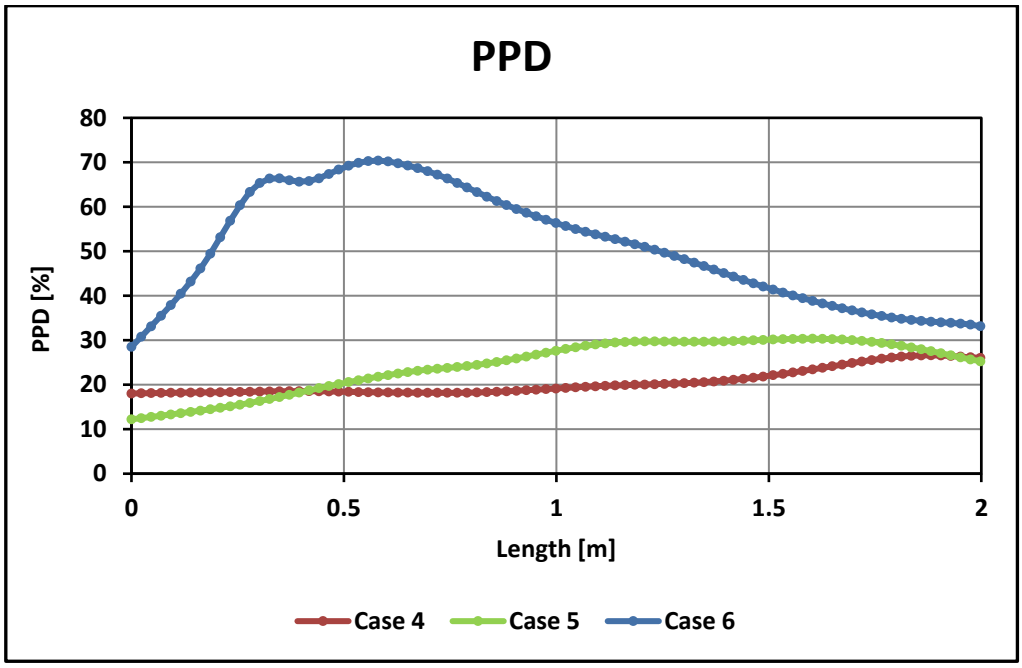

Figure 28 Chart Shows the PPD % at Line Probe

4.2.3 Local Air Quality Index (LAQI)

The elimination of pollutants after adjusting the outlet place at the level of the head is seen as supplementary and effective due to the removal of pollutants emanating speed from the patient's mouth directly towards the outlet. The values were found from Figure 29 (a), at 9 ACH is around 5 LAQI in the HCW area, while is 0 LAQI in the area behind HCW close to the corner. Figure 29 (b) For 12 ACH, the values are excellent except for the HCW area, which is still exposed to contamination. As for 15 ACH Figure 29 (c), the area is generally clean thanks to the strong airflow and the outlet placement, as mentioned by Ameer *et al*. (2021).

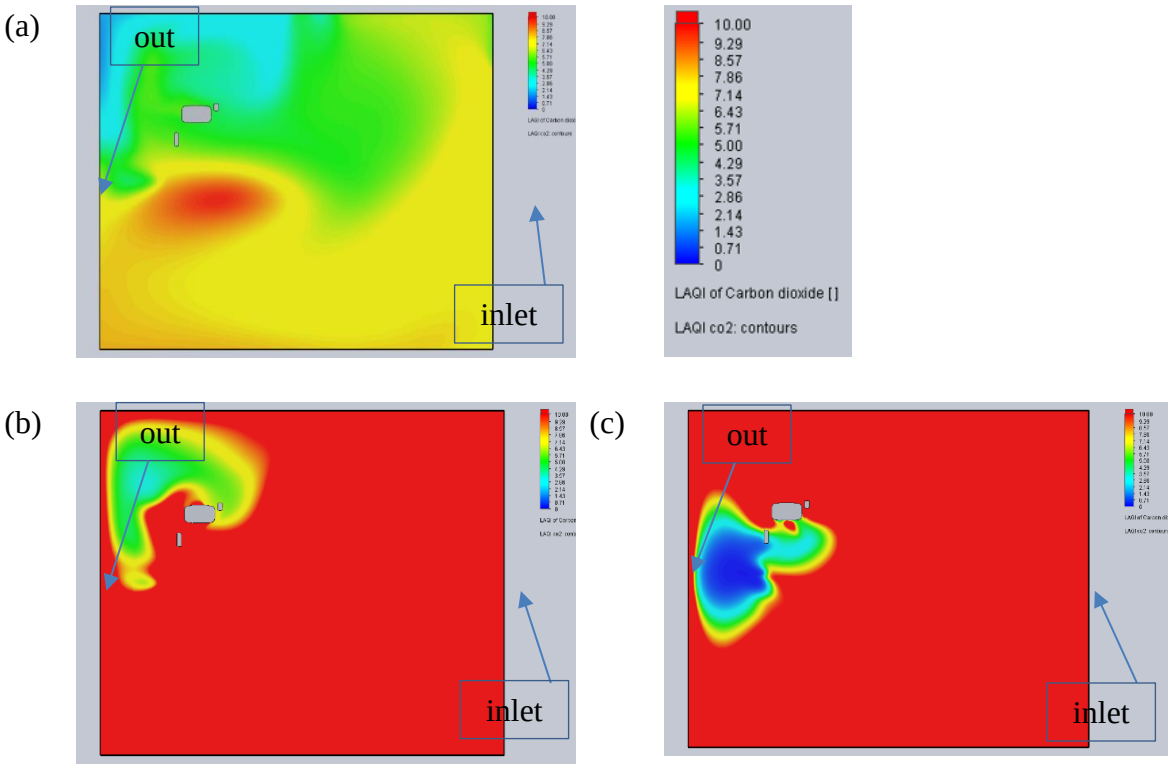

Figure 29 Top view for LAQI OF CO_2 (a) Case 4 at 9 ACH (b) Case 5 at 12 ACH (c) Case 6 at 15 ACH

4.2.4 Trace Study of CO_2 (Flow Trajectories)

Removal of pollutants must consider not only the pollutant's concentration but also the fluid's pressure gradient. These characteristics can be determined from equation 3.15. The simulation results were shown at 9 ACH (Figure 30 (a)). The presence of contaminants is 0.0005 ppm behind the HCW, which is considered a high value. From Figure 30 (b) at 12 ACH, it could be seen that the concentration decreases in the same area to 0.0003 ppm. On the opposite point near the outlet, the value goes up until it exceeds 0.001 ppm due to the source of CO_2 being near the outlet. On the contrary, as shown in Figure 30 (c), for 15 ACH, almost all concentrations within the room are less than 0.0001 ppm except for the area above the bed. This results from the velocity being related to diffusion according to equation 3.15.

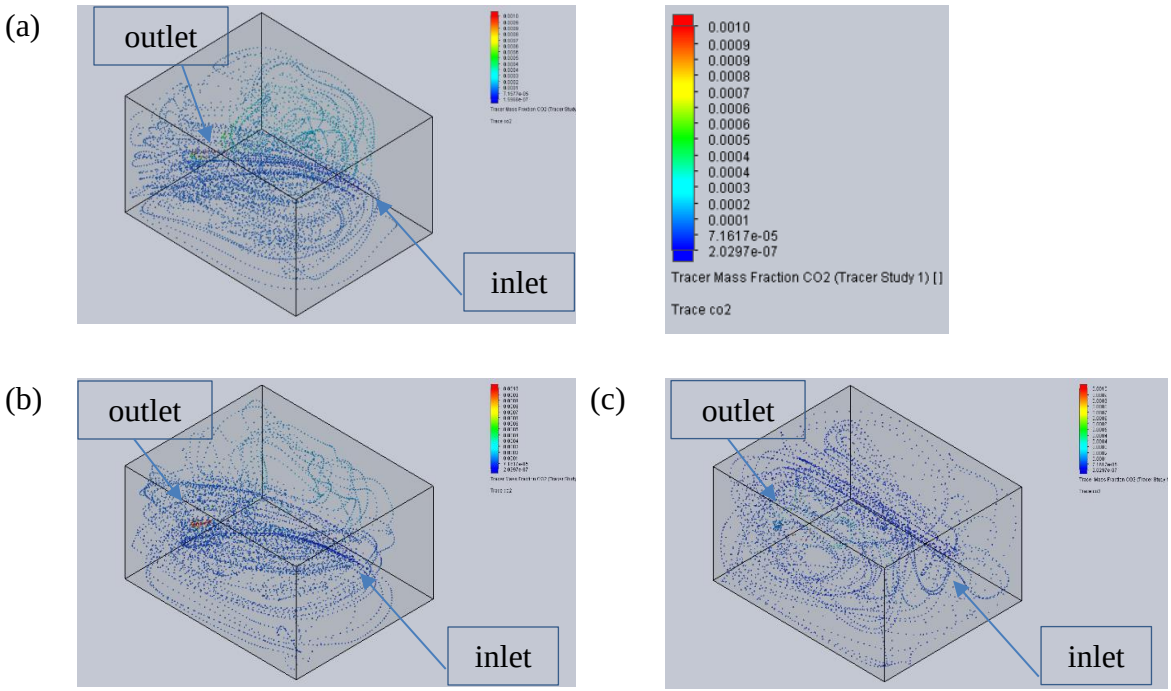

Figure 30 : Flow Trajectories for Trace study of CO_2 (a) Case 4 at 9 ACH (b) Case 5 at 12 ACH (c) Case 6 at 15 ACH

4.2.5 Turbulence Intensity

The modeling shows that the turbulence intensity values slightly fluctuate nearby the location of the outlet. By comparison between Figure 24 (a) and Figure 31 (a) at (9) ACH, it was found that both have similar values in the occupied zone. However, there is a variance in the value at the corners of the room, especially at the outlet location. Looking at the top view in Figure 31 (d), it is noticeable that the presence of high-intensity values on the opposite side of the HCW, which, as per Anthony & Nath Verma (2021), is not adequate for achieving thermal comfort. For 12 ACH (Figure 31 (b & e)), the outcomes improved even though there are some high turbulence intensity areas at the bed's surround due to increased mixing. At 15 ACH (Figure 31 (c & f)), turbulence intensity is formed on the opposite side of the HCW, and the right side of the HCW also has a high value. While from the frontal view of Figure 31 (c), in the middle of the room, it appears that there are regular intensity

values except for the bed edge, which exceeds 40%. The turbulence intensity behaves similarly to the flow velocity (Cao *et al*., 2011). According to the following chart Figure 32, there are no significant differences between 9, and 12 ACH, with the most significant difference being 10% in the middle of the bed area. For 15 ACH, there was a significant change in the value that reached up to 60% for the first part of the occupied area close to the outlet. As a result of the impact of the inlet airflow, which causes emerging turbulent waves. The final flow (15 ACH) should be avoided in this design since it causes discomfort because the turbulence intensity is 30% and higher, which is not desired as per Ležovič *et al*. (2013).

(a)

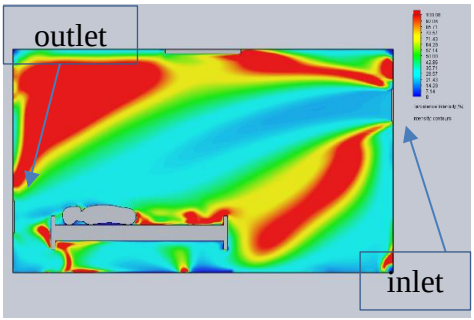

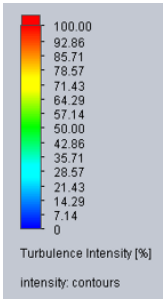

(b)

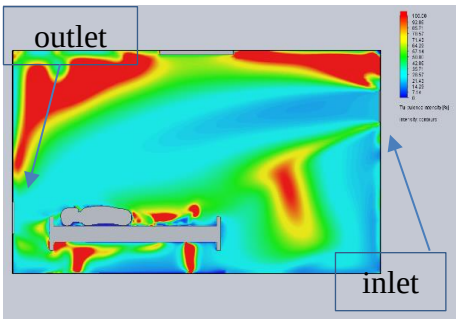

(c)

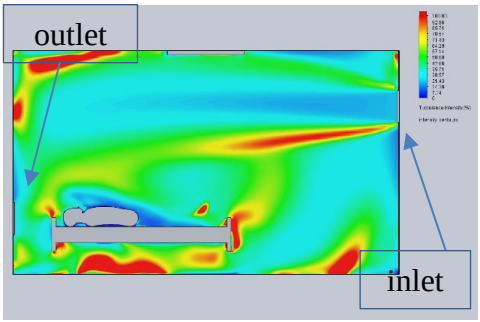

(d)

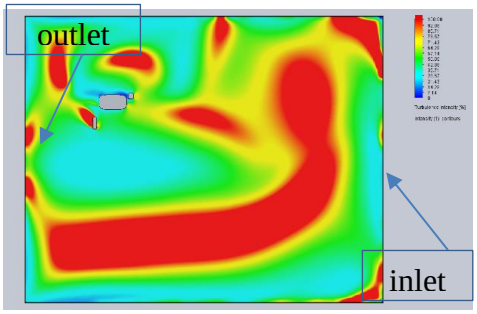

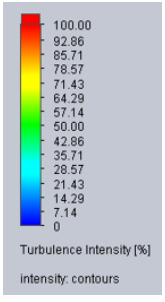

(e)

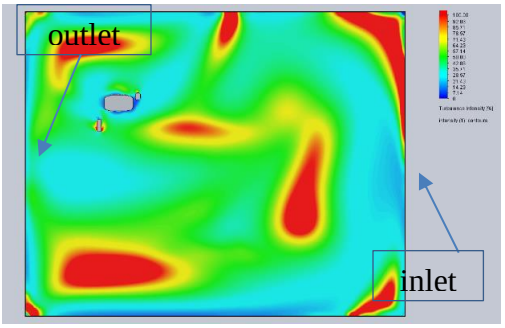

(f)

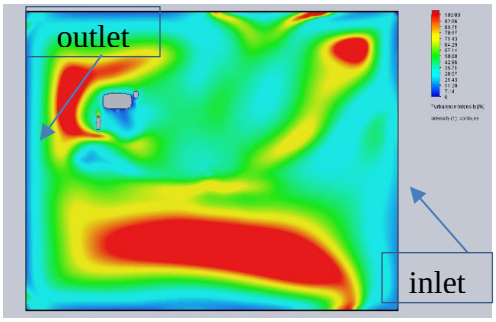

Figure 31 : Front View for Turbulence Intensity (a) Case 4 at 9 ACH (b) Case 5 at 12 ACH (c) Case 6 at 15 ACH. Top View (d) Case 4 at 9 ACH (e) Case 5 at 12 ACH (f) Case 6 at 15 ACH

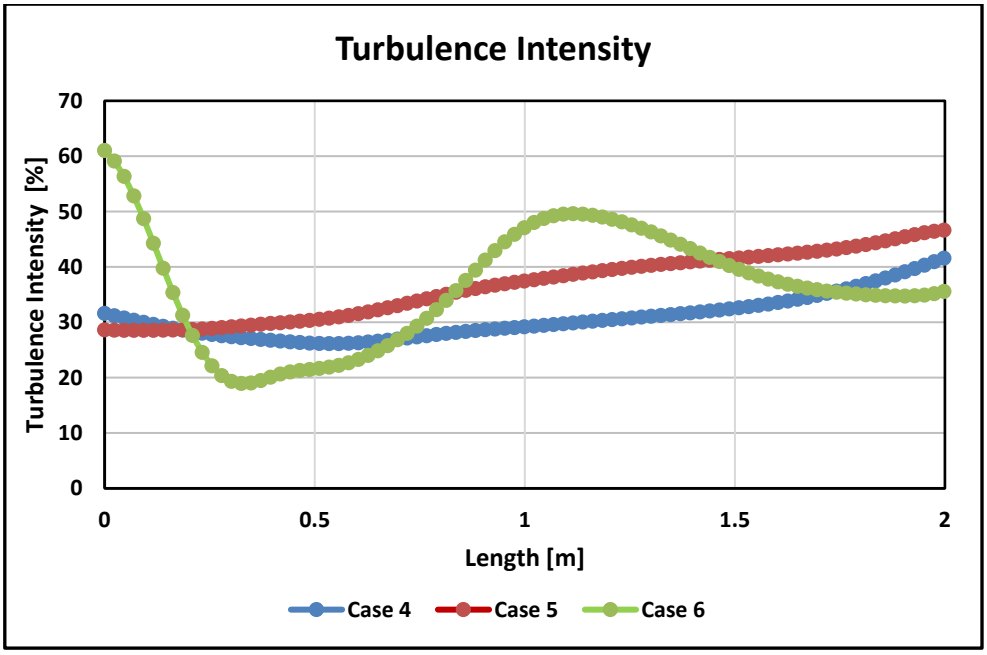

Figure 32 : Chart Shows the Turbulence Intensity at Line Probe

4.2.6 Contaminant Removal Effectiveness & Air Diffusion Performance Index (CRE) & (ADPI)

In this design, it's noticeable that the value of CRE is increased unexpectedly due to the proximity of the outlet to the mouth's patient, corresponding to Eldegwy *et al*. (2015), and owing to the flow, especially for 12 ACH. Whereas at 15 ACH, the results were higher

as the air pushed the pollutants toward the outlet. Regarding the ADPI, the optimum recommended by Rusly *et al*. (2014), the value should be more than 80% which means it's achieved through 12 and 15 ACH.

Table 5

CRE & APDI Values for Cases 4, 5, and 6

	9 ACH	**12 ACH**	**15 ACH**
CRE	5.32	15.41	7.53
APDI %	73.0	80.3	87.6

4.3 RESULTS OF CASES 7, 8, AND 9

Exhaled flow, ventilation, and other factors increase the dispersal of airborne contaminants inside a space (Liu *et al*., 2019). Therefore, a suitable design is required. The ventilation system design shown in Figure 4 was chosen. In this design, the inlet was seated at the top of the wall behind the HCW at a distance of 0.5 m from the roof, and the outlet was located on the bottom, close to the floor on the other wall's side at a distance of 0.5 m.

4.3.1 Predicted Mean Vote (PMV)

Charts will be used to display the results, which depend on a line drawn at a vertical distance of 1 m from the ground and is parallel to the patient through a distance of 2 m, as shown in Figure 18. Figure 33 (a & d) at 9 ACH shows that the predominant feeling is warmth with a value of 1.29 PMV. Except for the occupied area, where the value is found to be high between 2 to 3 PMV, the area suffers from a hot feeling. This is because bodies generate heat. The normal thermal exists in the room border beside the wall on the side of the patient's head and the airflow path. In addition, the green space exists at a low level owing to the decreases in air path gradually from the outlet to the other end, as the air hits the wall

and returns to the opposite side (inlet side) see Figure 33 (a). While at 12 ACH (Figure 33 (b & e)), it is clear that the green space increases only on the border of the room, as is shown in the top view Figure 33 (e). As air hits the opposite wall, it spreads gradually toward the center. Furthermore, from Figure 33 (b), it is noticeable that the green area has increased as a result of the increase in airflow, despite existing of some hot regions on the roof. Raising the airflow until 15 ACH significantly reduces the warm and hot region, as Figure 33 (c) illustrates. However, again the occupied area is still suffering from the warmth, as is evident from the top view in Figure 33 (f), due to the inlet being located higher than the occupancy level, where it throws the air away toward the opposite side.

(a)

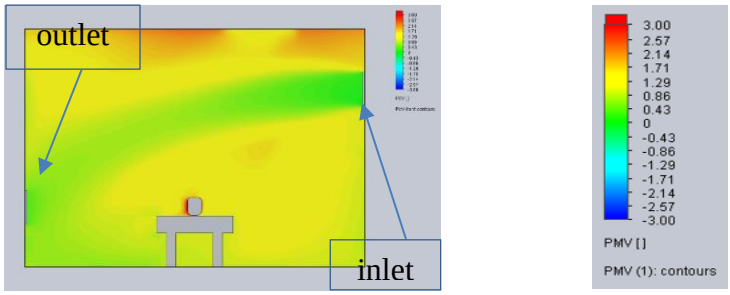

(b)

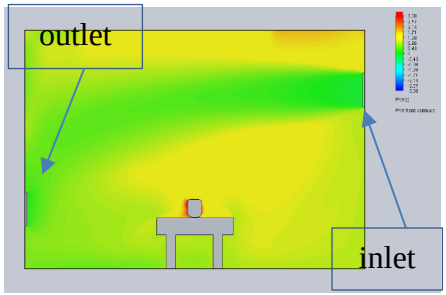

(c)

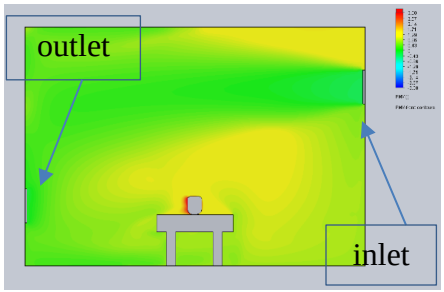

(d)

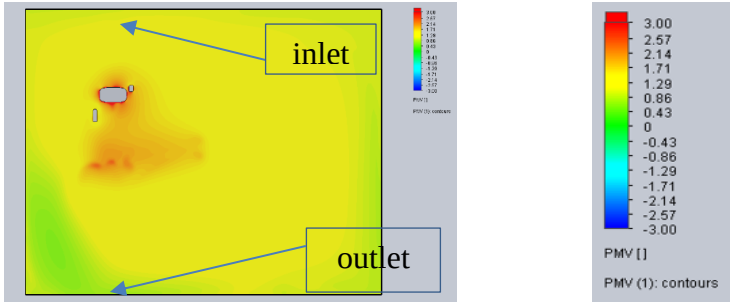

(e)

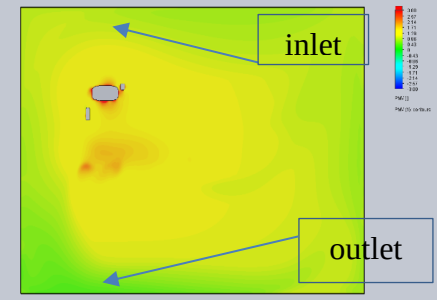

(f)

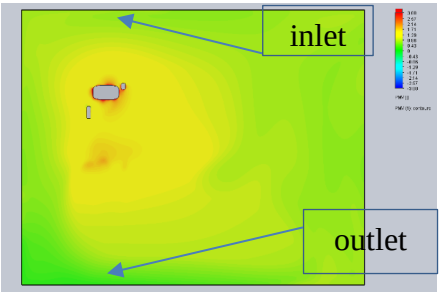

Figure 33 : Front View for PMV (a) Case 7 at 9 ACH (b) Case 8 at 12 ACH (c) Case 9 at 15 ACH. Top View (d) Case 7 at 9 ACH (e) Case 8 at 12 ACH (f) Case 9 at 15 ACH

4.3.2 Predicted Percent Dissatisfied (PPD)

The results are similar to the results of PMV. For 9 ACH (Figure 34 (a)) shows that the occupied place has a value of more than 43% PPD. This number is present in a considerable portion of the room and diminishes as airflow speed increases. It is clear from Figure 34 (b & c) for 12 and 15 ACH, the area surrounding the occupied area has a value starting from 20-25% PPD and goes up after becoming far from the inlet effect. The chart below (Figure 35) illustrates that the increase in airflow has a positive effect on thermal comfort, where the values of PPD are reduced by half from 9 to 15 ACH. However, the occupied region still has high values of PPD.

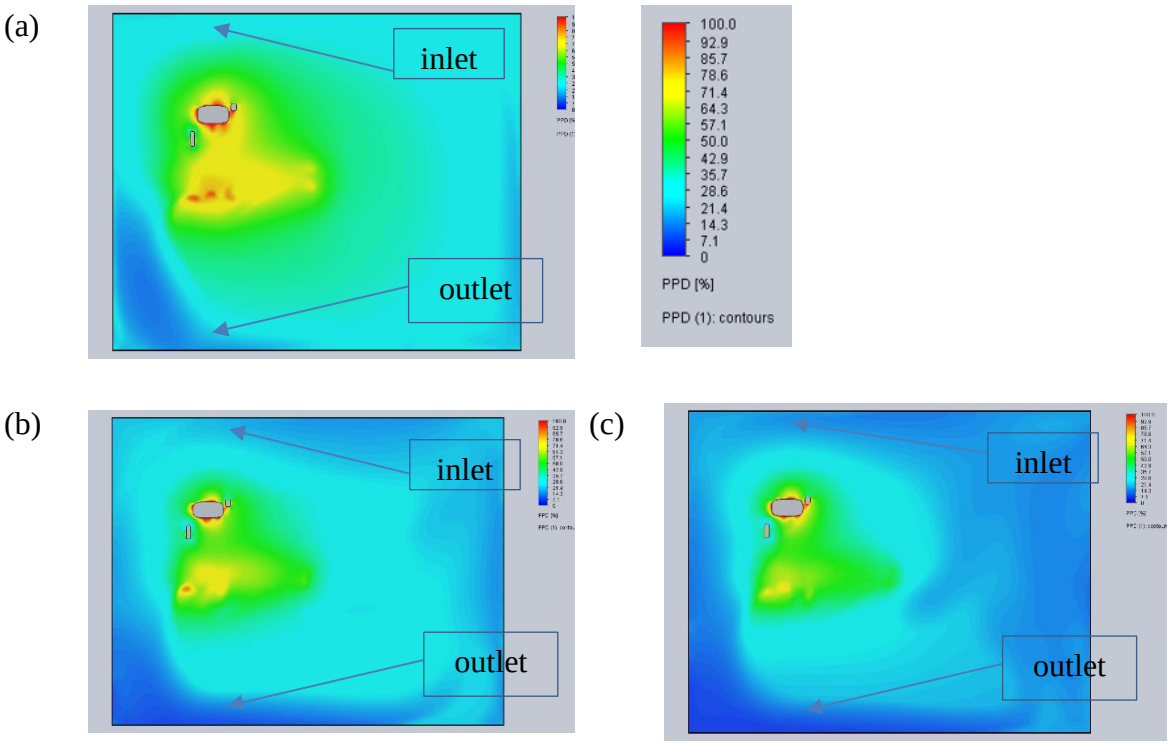

Figure 34 : Top view for Fluid PPD (a) Case 7 at 9 ACH (b) Case 8 at 12 ACH (c) Case 9 at 15 ACH

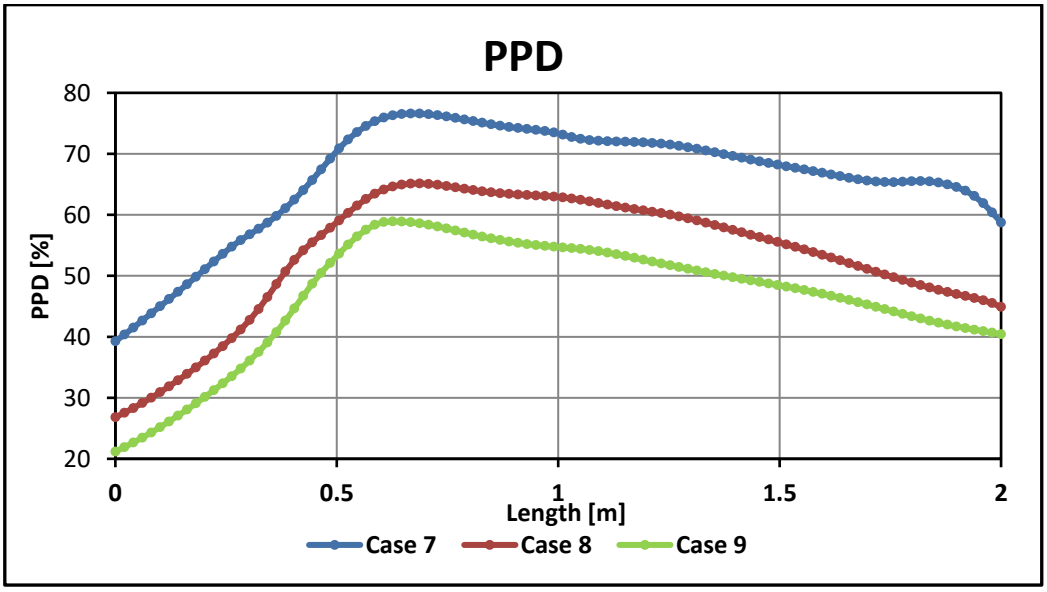

Figure 35 : Chart Shows the PPD % at Line Probe

4.3.3 Local Air Quality Index (LAQI)

The placement of the inlet and outlet is a significant factor in determining how well pollutants are eliminated (Ameer *et al*., 2021). Figure 36 (a) for 9 ACH shows that the area of minimum contamination appears on the right side of the HCW. However, the region as a whole is still exposed to pollution due to the air pushing pollutants and not pulling them directly. While at 12 ACH (Figure 36 (b)), although the situation has improved in removing contaminants, there is still some spread toward the unoccupied region because the air path is directing the pollutants. It seems that the air velocity wasn't sufficient to remove the pollutants effectively. As for 15 ACH (Figure 36 (c)), it appears the best flow for this design in eliminating pollutants owing to the force of the air.

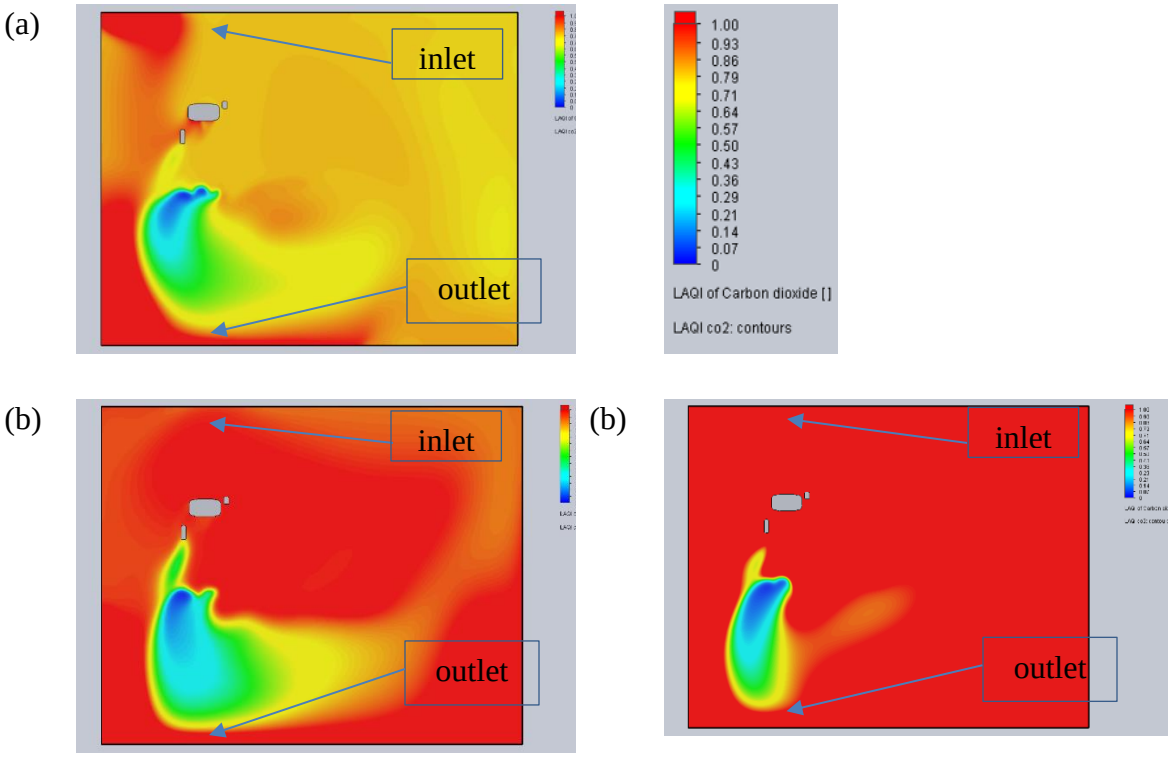

Figure 36 : Top view for LAQI OF CO_2 (a) Case 7 at 9 ACH (b) Case 8 at 12 ACH (c) Case 9 at 15 ACH

4.3.4 Trace Study of CO_2 (Flow Trajectories)

Figure 37 (a) at 9 ACH shows that the concentration of pollutants is reduced in the air path between the inlet and the outlet, which helps to ensure a clean area. The concentration near the patient is 0.0005 ppm. Nevertheless, the rest of the room has a concentration of approximately 0.0018 ppm, which corresponds with the Local Air Quality Index (LAQI) outcomes. For 12 ACH (Figure 37 (b)), the results show the area far from the ventilation pathway has a slightly lower concentration, about 0.0011 ppm. As for 15 ACH (Figure 37 (c)), the efficiency was improved, where the values became approximately 0.00007 ppm for the unoccupied region.

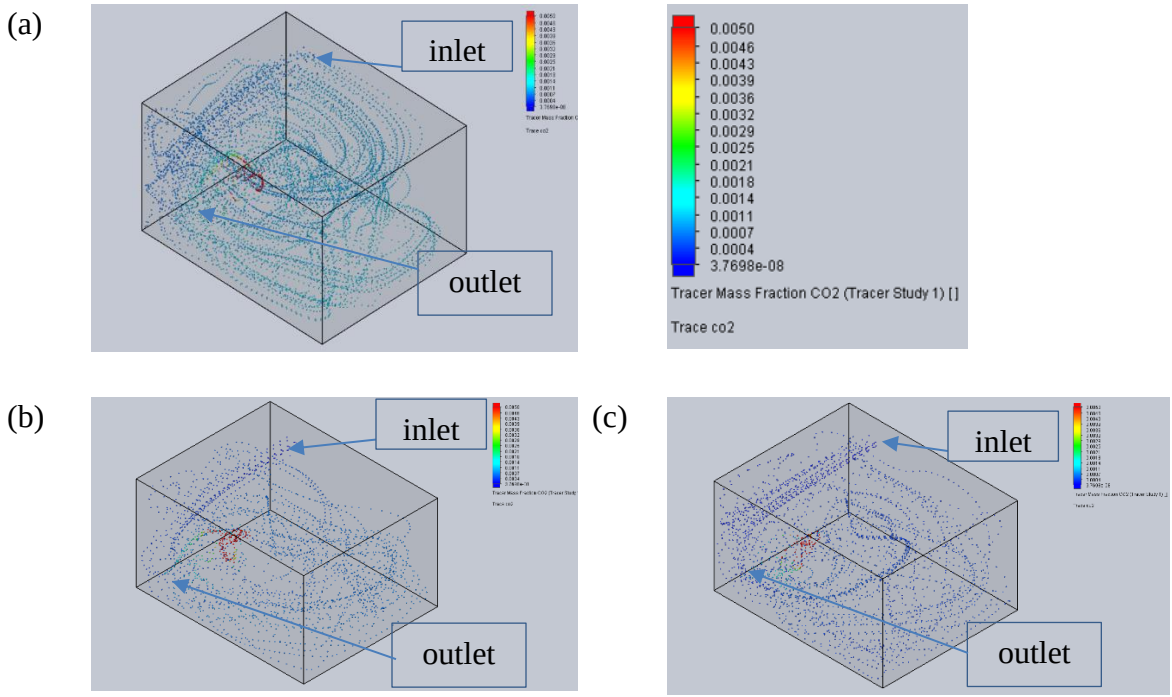

Figure 37 : Flow Trajectories for Trace study of CO_2 (a) Case 7 at 9 ACH (b) Case 8 at 12 ACH (b) Case 9 at 15 ACH

4.3.5 Turbulence Intensity

The airflow is affected by the location of the openings, which in turn impacts the turbulence intensity. As seen from Figure 38 (a) at 9 ACH, HCW and the patient's body are preventing air passage. It shows the severe turbulence around this area (bodies area) (Cheng *et al*., 2021). Therefore, turbulence formed after the bodies. Then the air mixing happened on the opposite side of HCW, which explains the high value of turbulence intensity there. For 12 ACH, Figure 38 (b) demonstrates the results became logical in the occupied area. However, the high turbulence intensity is concentrated in the outlet region, except for the surrounding area beside the walls. Similar results are found in Figure 38 (c) at 15 ACH as a result of the force of air, which leads to the air being reflected from the wall where the outlet is located; therefore, high turbulence intensity approaches the occupied area. As shown in Figure 39, the beginning of the bed is 0 - 0.5 m and has good results for 9 and 12 ACH, then all go up until they reach high and undesirable numbers of intensity in ventilation designing.

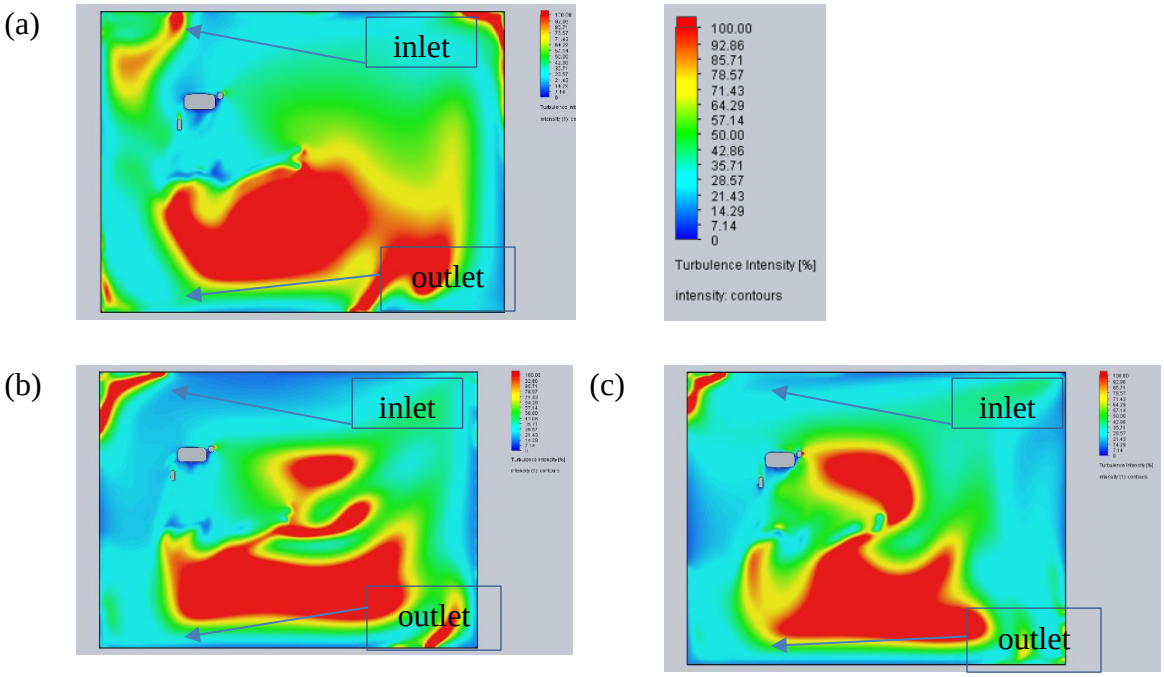

Figure 38 : Top View for Turbulence Intensity (a) Case 7 at 9 ACH (b) Case 8 at 12 ACH (c) Case 9 at 15 ACH

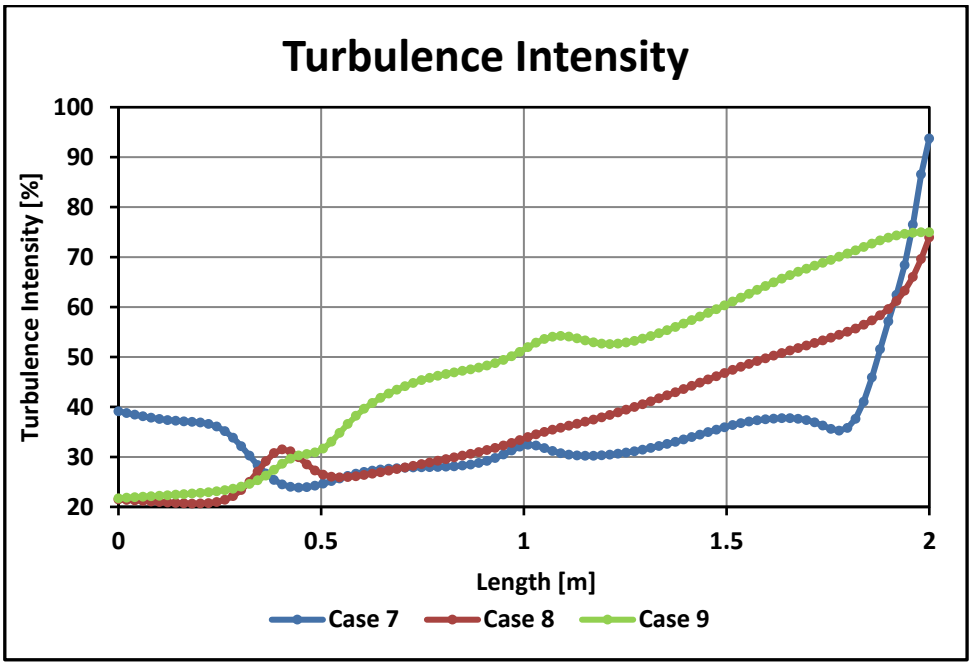

Figure 39 : Chart Shows the Turbulence Intensity at Line Probe

4.3.6 Contaminant Removal Effectiveness & Air Diffusion Performance Index (CRE) & (ADPI)

As a result of the decrease in the values in the LAQI, the effectiveness of the results of pollutant removal appeared less than in the other designs, where at 9 ACH has a low value. However, the values for 12 and 15 ACH are acceptable as they are more than 1 CRE. According to APDI, both 12 and 15 ACH have achieved decent air diffusion performance according to the diffusers' location and due to the distances between the diffusers (Rusly *et al*., 2014), excluding 9 ACH owing to the feebleness of the airflow all results are existing in (Table 7).

Table 6
CRE & APDI Values for Cases 7, 8, and 9

	9 ACH	12 ACH	15 ACH
CRE	0.84	1.01	1.52
APDI %	72.4	80.3	85.0

4.4 RESULTS OF CASES 10, 11, AND 12

While the preceding three simulations' designs were somewhat similar, this last one is unique. Both open are roof-mounted in this design the distance from the side wall is 1 m for the inlet and 0.5 m for the outlet as shown in Figure 5.

4.4.1 Predicted Mean Vote (PMV)

Figure 40 (a) depicts the front view at 9 ACH, where the green zone covers the area below the patient level. After that, the value of PMV gradually increases until it reaches 1.3 PMV, where the feeling of warmth is dominant owing to the buoyancy factor. When the airflow is increased to 12 ACH (Figure 40 (b)), similar results were revealed, but with a more noticeable green area due to the increasing added air. The warmth area gradually declines in the occupied zone. Therefore, an increase in airflow improves thermal comfort. However, at 15 ACH (Figure 40 (c)), the upper region is still uncomfortable thermally because the airflow is not directed and cannot reach that area.

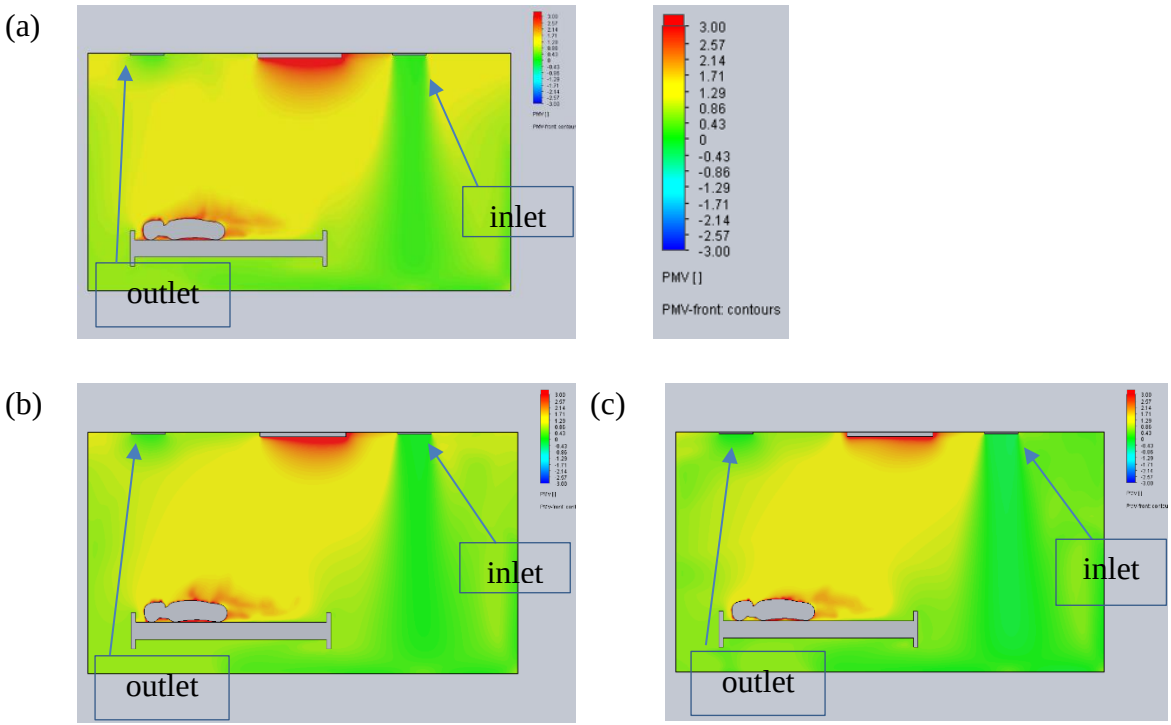

Figure 40 : Front view for PMV (a) Case 10 at 9 ACH (b) Case 11 at 12 ACH (c) Case 12 at 15 ACH

4.4.2 Predicted Percent Dissatisfied (PPD)

Since temperature is integral to the description of PPD, thermal dissatisfaction produces outcomes similar to thermal prediction. It can be shown from Figure 41 (a) at 9 ACH, thermal discomfort starts to clear out of the air path, and it slowly rises. Especially in the space where the patient and the HCW are located, as the predominant value is 50%, which consider a high value (Karimipanah *et al*., 2012). The bed works as a barrier preventing the air from reaching the upper region, dispersing the air to the sides. For 12 and 15 ACH (Figure 41 (b & c)), a decrease in thermal discomfort is detected on the inlet side, and the results are considered highly satisfactory. However, the occupied area is still not affected by the new air. As shown from the chart below (Figure 42), it is clear that thermal dissatisfaction exists

in the occupied area, where the value ranges between 18-55%. In light of this, the design is thermally inefficient and should be revised.

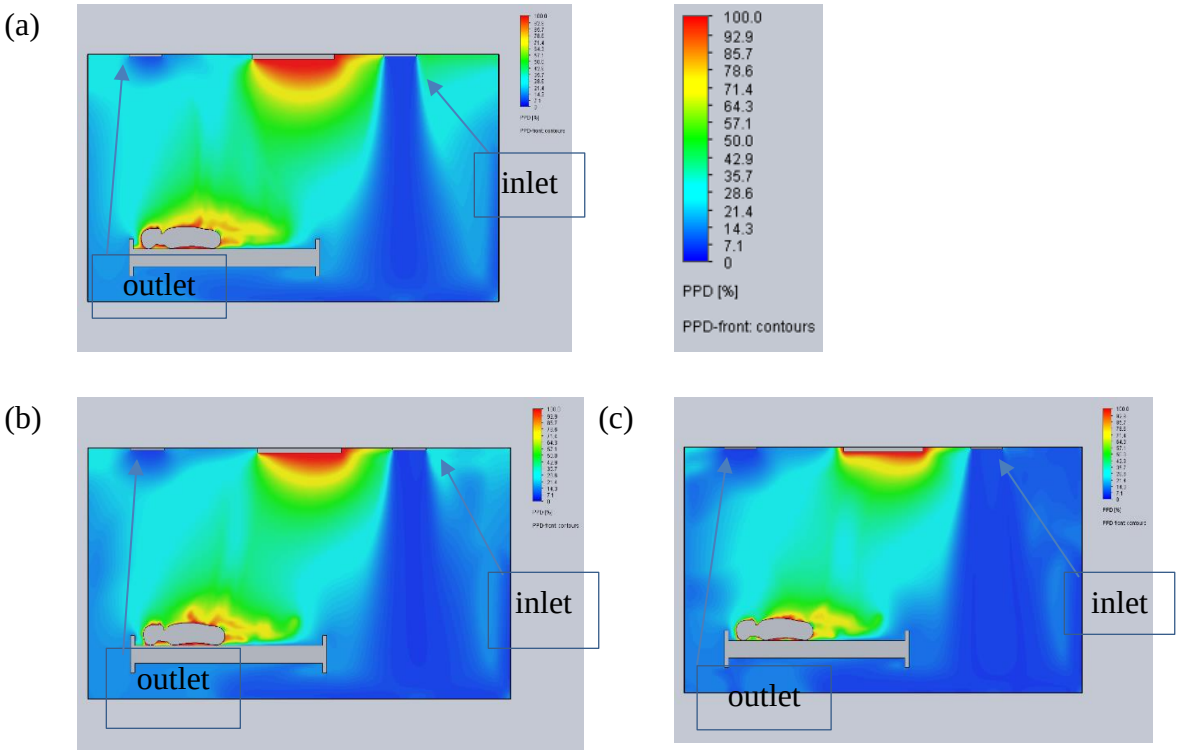

Figure 41 : Front view for Fluid PPD (a) Case 10 at 9 ACH (b) Case 11 at 12 ACH (c) Case 12 at 15 ACH

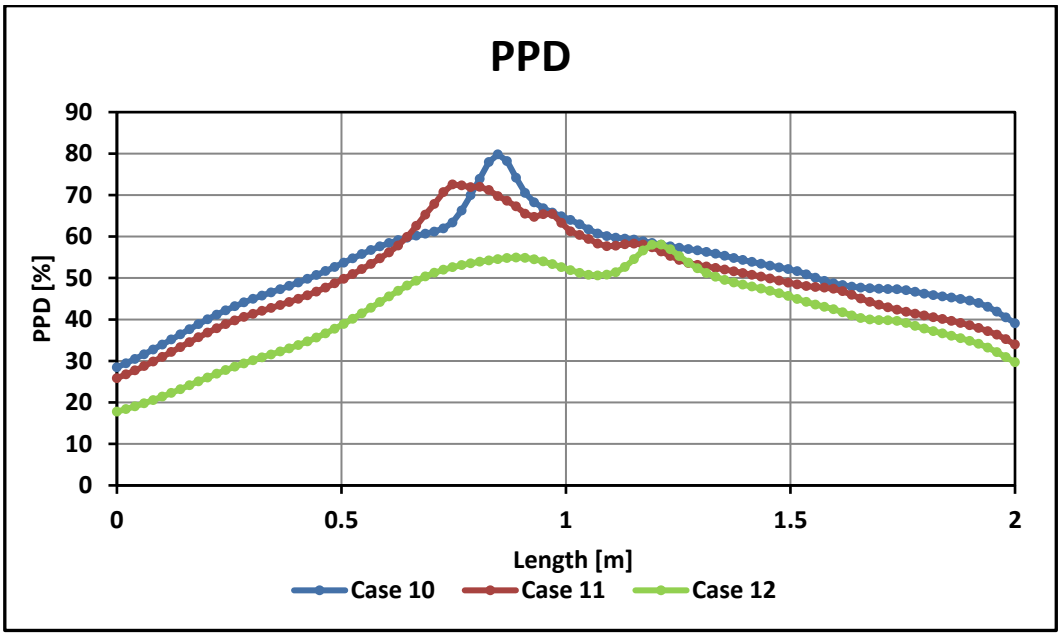

Figure 42 : Chart Shows the PPD % at The Line Probe

4.4.3 Local Air Quality Index (LAQI)

As illustrated in Figure 43 (a) for 9 ACH, the outlet absorbs contaminants emitted from the patient's mouth, but some fall down due to gravity and are stuck in the lower level. At the same time, Figure 43 (b) at 12 ACH results show that the increase in the airflow is noticed and led to more polluted regions. At 15 ACH (Figure 43 (c)), the contaminated area is confined near the inlet region towards the working area. A correlation between airflow and pollution levels is visible.

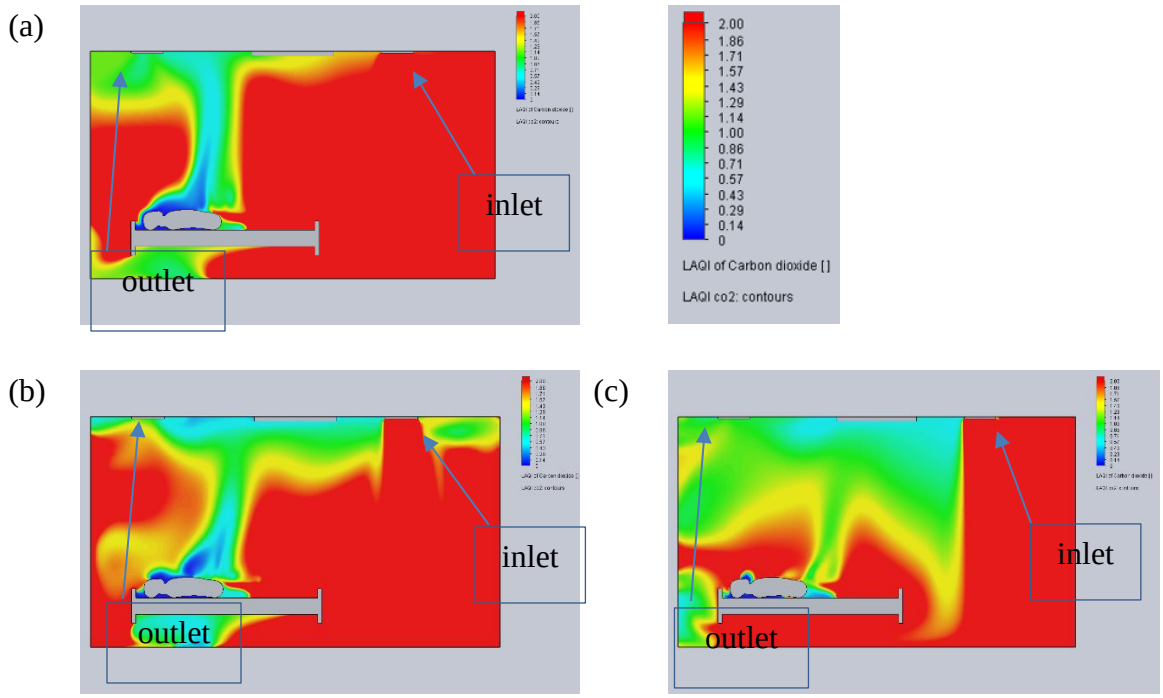

Figure 43 : Front view for LAQI OF CO_2 (a) Case 10 at 9 ACH (b) Case 11 at 12 ACH (c) Case 12 at 15 ACH

4.4.4 Trace Study of CO_2 (Flow Trajectories)

At 9 ACH, it can be seen from Figure 44 (a) where the pollutants are present at a high concentration of 0.005 PPM at the location of their source (mouth's patient), then it gradually decreases towards the outlet. As shown in Figure 44 (b) at 12 ACH, the mixing of pollutants increases, which helps to spread their concentration over a larger volume. The airflow increase affects the contaminants due to the distribution of these pollutants around the space, as declared in the previous paragraph on the Local Air Quality Index (LAQI). While at 15 ACH from (Figure 44 (a)), the airflow force made the unoccupied zone a barrier that forces the pollutants to be just in the occupied zone. Referring to that inlet location in this design, removing the contaminants is considered inappropriate.

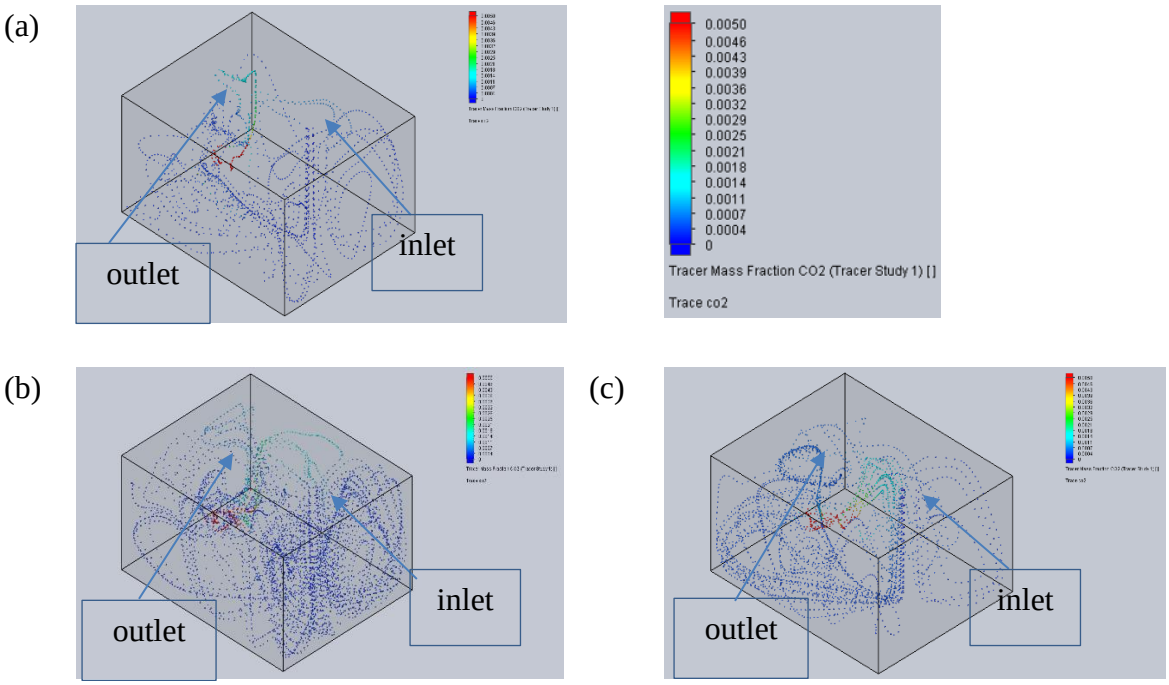

Figure 44 : Flow Trajectories for Trace study of CO_2 (a) Case 10 at 9 ACH (b) Case 11 at 12 ACH (c) Case 12 at 15 ACH

4.4.5 Turbulence Intensity

The occupied area has high turbulence intensity, as shown in Figure 45 (a & d). For 9 ACH, the values are between 25-50% near the patient's head. After that, there is a fluctuation in the bed area. However, the room has huge values of intensity that are distributed around the room. At 12 ACH (Figure 45 (a & d)), it is evident that a greater volume of airflow was pushed away from the patient's head due to the reflection of air on the wall behind the patient. This caused the region of turbulence to move away too, which made the value drops to 25% in the same area. The chart in Figure 46 shows the intensity values above the bed. As it is clear from Figure 45 (c), for 15 ACH at 0-0.75 m, the values are in the range of 20-30%. Generally, the area has high-intensity values concerning the top view Figure 45 (f). While at 12 ACH in 0.75-1.5 m, the values are again around 20-30%. While for 9 ACH between 0.75-

1.25 m, the values are between 15-35%. Due to the fluctuations and the high values, the three cases might not be considered good designs.

(a)

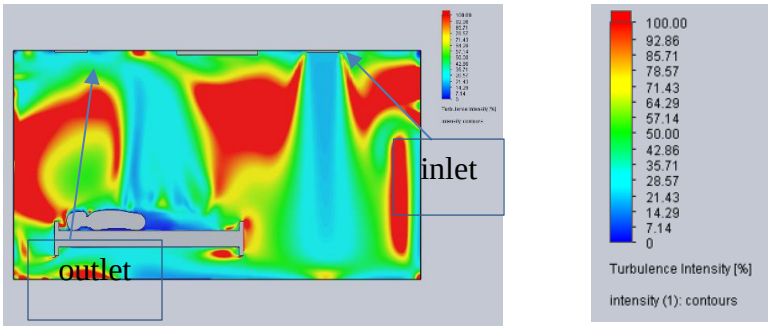

(b)

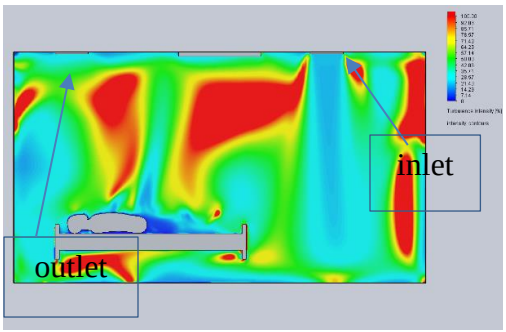

(c)

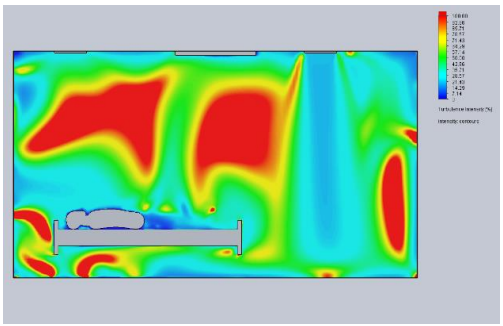

(d)

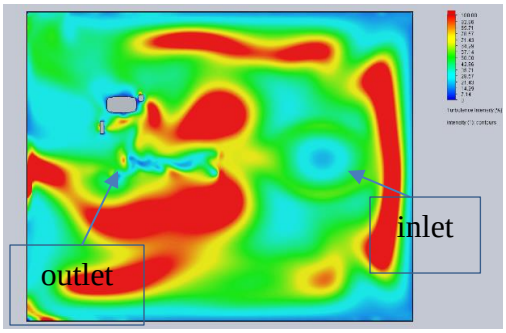

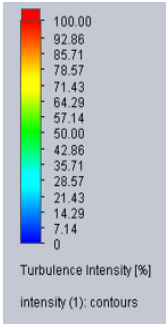

(e)

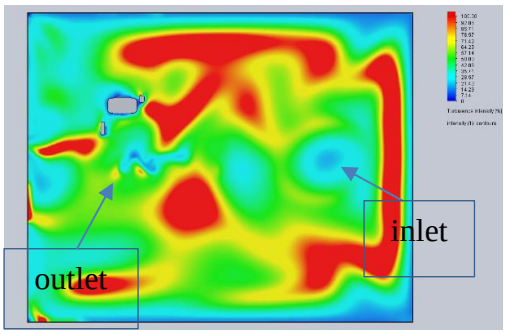

(e)

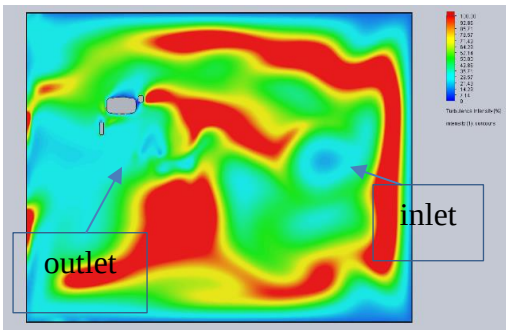

Figure 45 : Front View for Turbulence Intensity (a) Case 10 at 9 ACH (b) Case 11 at 12 ACH (c) Case 12 at 15 ACH. Top View (d) Case 10 at 9 ACH (e) Case 11 at 12 ACH (f) Case 12 at 15 ACH

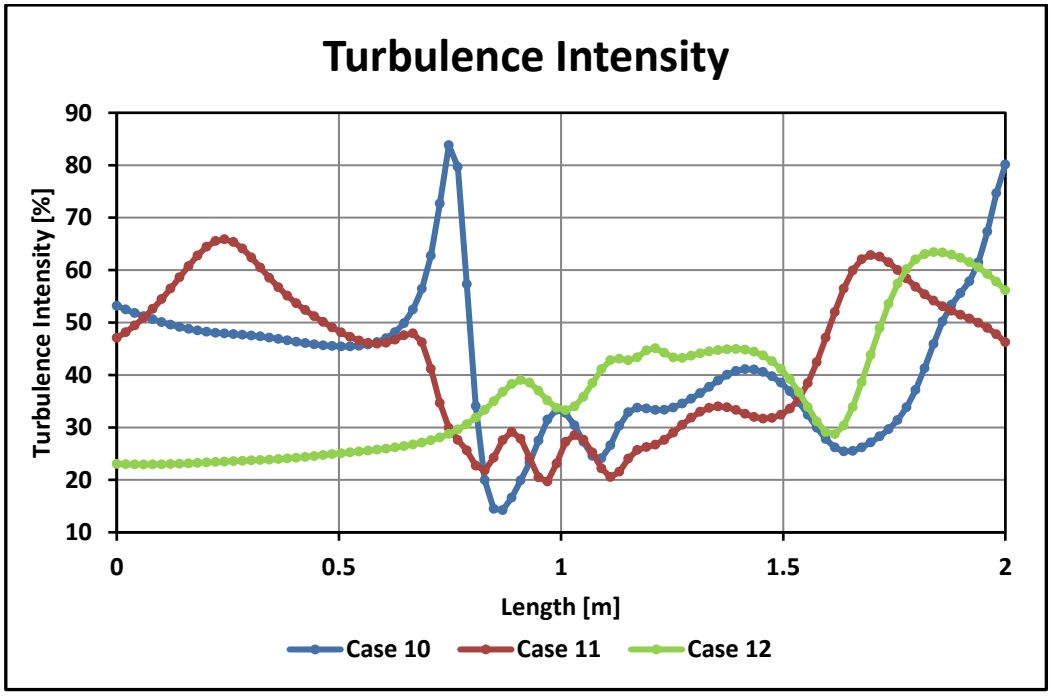

Figure 46 Chart shows the Turbulence Intensity at The Line Probe

4.4.6 Contaminant Removal Effectiveness & Air Diffusion Performance Index (CRE) & (ADPI)

As per pollutant removal results, 9 ACH classifies as the finest due to the lack of severe mixing of pollutants, followed by 12 and 15 ACH, respectively. Besides, all the values of CRE are more than 1. This means that the ventilation system is still effective in removing contaminants, as ADPI is based on on-air velocity and effective draft temperature (Ahmed, 2012). These two cases are more than 80%; the highest value was 12 ACH, followed by 15 ACH, then 9 ACH. However, this is considered close to the adequate limit.

Table 7

CRE & APDI Values for Cases 10,11, and 12

	9 ACH	**12 ACH**	**15 ACH**
CRE	2.02	1.53	1.46
APDI %	78.1	82.6	80.7

4.5 SUMMARY OF THE RESULTS

Comparisons of the various designs and airflows thoroughly investigated are presented below. In the diagram in Figure 47, it can be noticed that cases 4, 5, and 6 (shown in Figure 3), where the outlet is situated close to the head at a low elevation, obtained effective removal of contaminants from the space compared to other designs. At the same time, a similar design (Figure 2) was used for cases 1, 2, and 3, where the outlet was situated above the patient's head, resulting in an undesirable outcome.

The efficiency of air diffusion, shown in the chart (Figure 48), shows how the values gradually increase with the airflow. Generally, for 15 ACH, all the cases are acceptable. For

12 ACH, reasonable outcomes were achieved, except for case 2, as the adequate limit is 80% APDI, which indicates the effect of airflow and the diffuser location on the outcomes.

Comparing the local air quality index by aeration value was found through the results in Figure 49 and Figure 50, illustrating the excellent values for pollutant removal efficiency. This shows the clear superiority for cases 4 and 5 except case 6, which has not had adequate results in a specific region at the beginning of the bed area where the contaminants' source exists. Owing to the direction of airflow becoming horizontal at 15 ACH, LAQI values rise dramatically to be equivalent to CRE values. The percentage of thermal dissatisfaction was compared for 9 ACH, as shown in Figure 52 (cases 1 and 4). The values were found to be between 18 and 30% PPD for the occupied area, which achieved beneficial results. While at 12 ACH, as it appears from Figure 53 (cases 2 and 5), it has similar results with some excesses for case 2 of more than 30%. However, for 15 ACH (Figure 54), it could be found that all the results at this airflow are undesirable owing to the direction of airflow not approaching the occupied area.

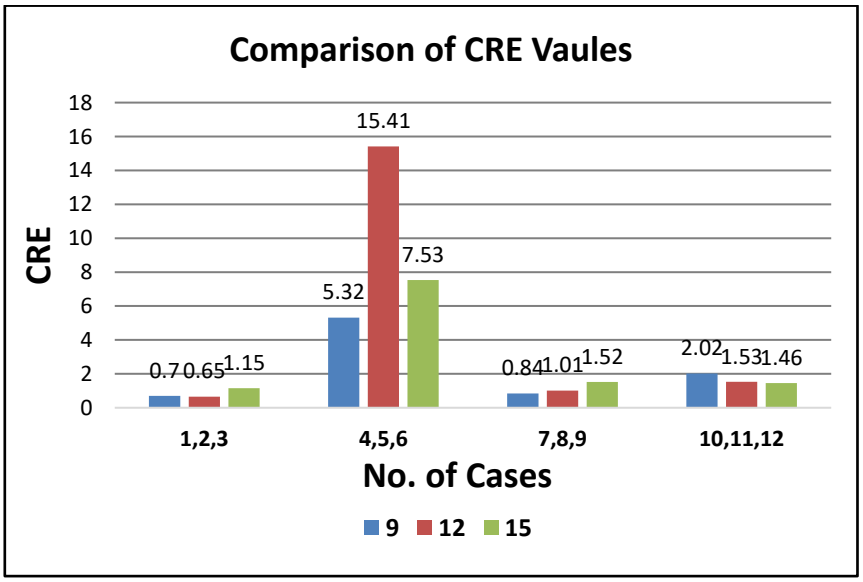

Figure 47 : Comparison of CRE Values

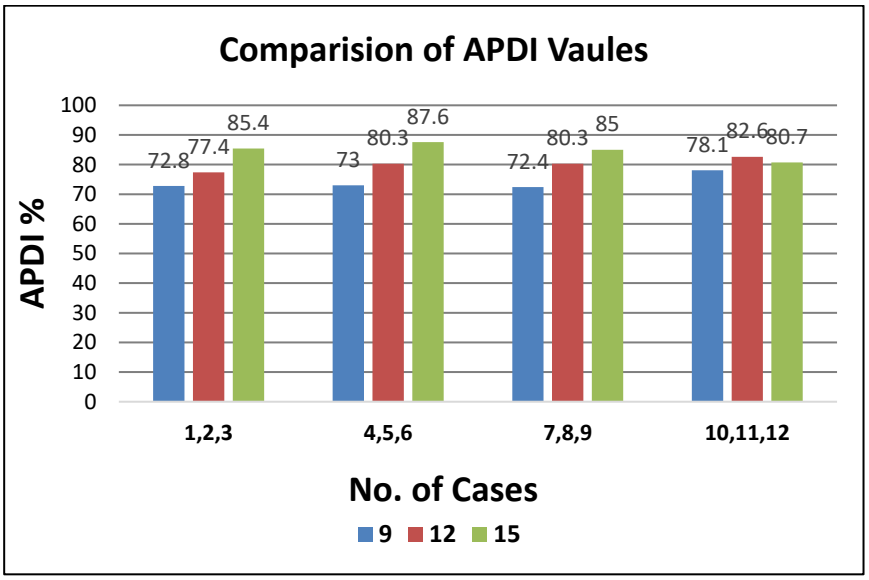

Figure 48 : Comparision of APDI Values

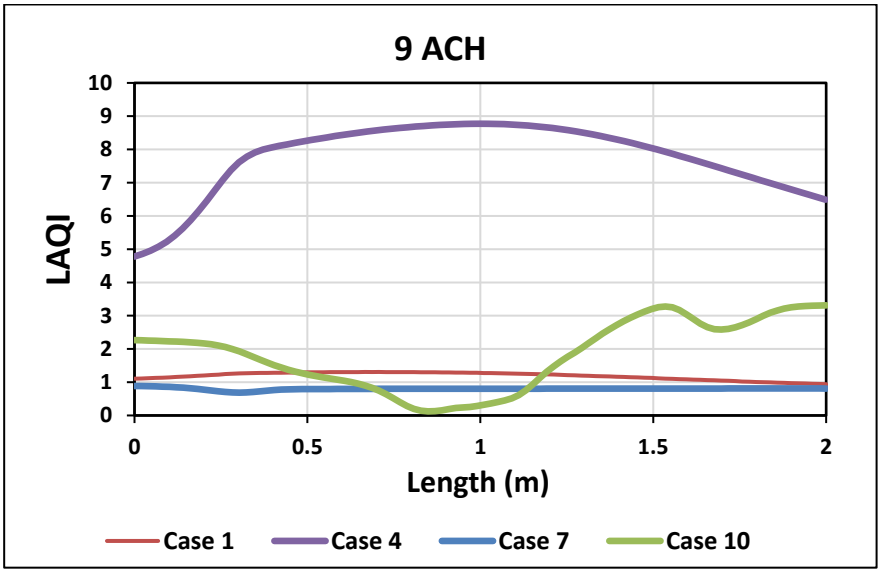

Figure 49 : Comparison of LAQI at 9 ACH

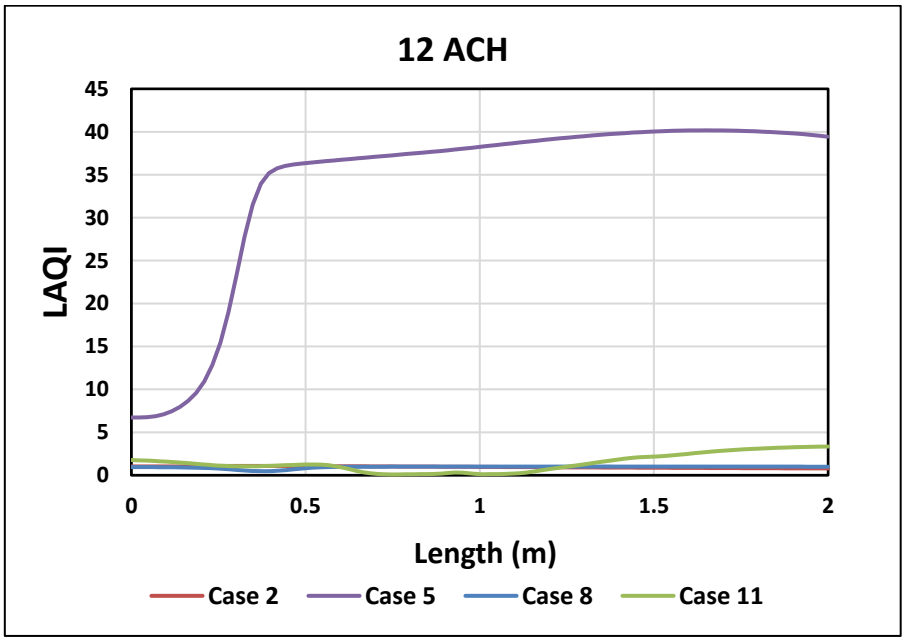

Figure 50 : Comparison of LAQI at 12 ACH

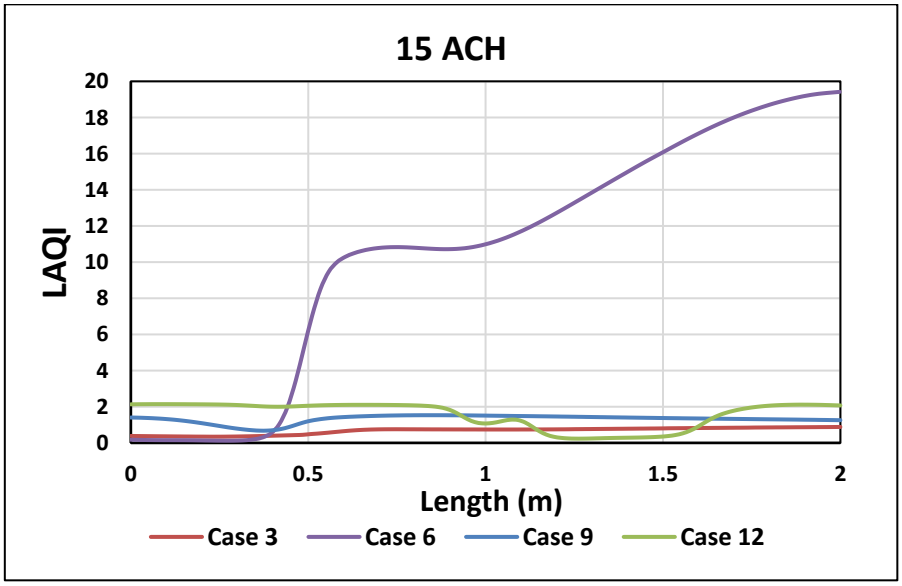

Figure 51 : Comparison of LAQI at 15 ACH

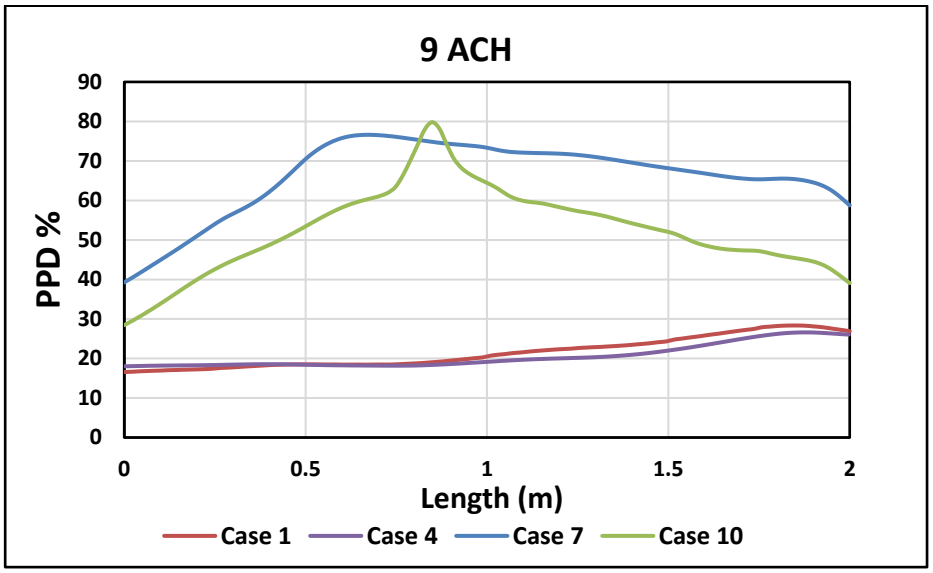

Figure 52 : Comparison of PPD % at 9 ACH

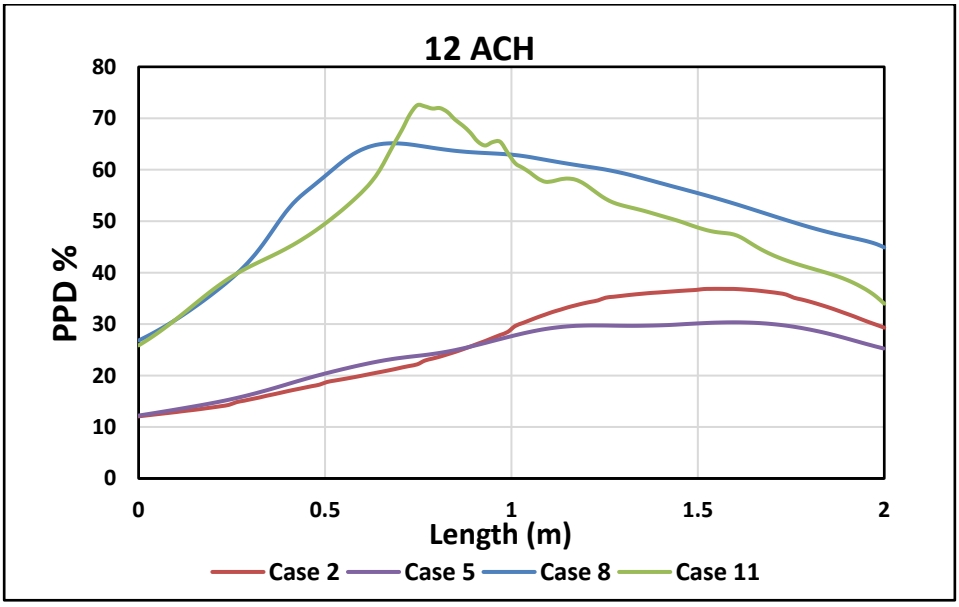

Figure 53 : Comparison of PPD % at 12 ACH

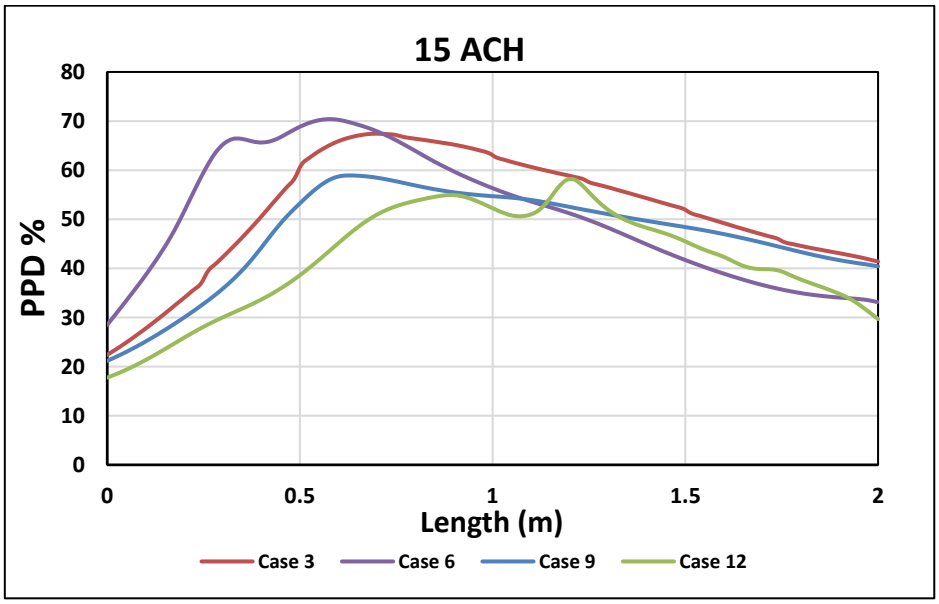

Figure 54 : Comparison of PPD % at 15 ACH

CHAPTER 5 CONCLUSIONS

5.1 SUMMARY AND CONCLUSIONS

This research, related to ventilation and air conditioning, was carried out due to its essential impact in every social building, especially in hospitals, as ventilation plays a significant role in human health and affects thermal comfort and the spread of pollutants like SRAS-Covid-19.

The first chapter covered a theoretical overview of thermal comfort, indoor air quality, the role of ventilation, and the locations of diffusers to achieve the research objective. While the referenced studies were presented in the second chapter, many boundary conditions were extracted from the previous studies and standards (ASHRAE), such as ventilation values, pressures, permissible temperatures, humidity, and diffuser arrangement. In addition, the representation of pollutants by carbon dioxide gas, the intensity, and the length of the turbulence were also discussed in detail.

In the third chapter, a detailed explanation has been performed in terms of the equations governing flow, turbulence, and the representation of pollutants, in addition to thermal satisfaction equations represented by PMV and PPD and pollutant removal by CRE and LAQI. Furthermore, this chapter presented model description, settings, and the choice of boundary conditions, while a mesh convergence study was also presented.

The final chapter of this research contains the current study's results: PMV, PPD, LAQI, flow trajectories (CO_2), turbulence intensity, CRE, and ADPI. Each result was discussed separately. A summary of the findings also indicates which design is preferable from the researcher's perspective. Results also revealed that an increase in airflow does not necessarily achieve a good environment that carries a minor amount of pollutants. However,

it has a positive effect on thermal comfort in some cases. Additionally, the arrangement of diffusers is essential for air distribution and affects thermal feeling.

The results have shown that cases 4 and 5 in the second design have the optimum value for removing the pollutants owing to the proximity of the outlet from the source of CO_2. Therefore, the contaminants are quickly removed. However, even though some cases were mildly acceptable, as for 9 ACH cases 1 and 4 and 12 ACH for cases 2 and 5, since the air was able to pass over the occupied area, it was found that all the designs, in general, did not provide a suitable thermal environment for the occupied area. However, the other cases are still not suitable for achieving thermal comfort.

5.2 THE LIMITATIONS OF THE MODEL, RECOMMENDATIONS AND FUTURE RESEARCH.

Even if there are numerous research studies in this domain, there is still a requirement to pursue a lot of work to find good designs. However, many difficulties remain during the modeling process, such as the model's size. In addition, it is difficult to create a proper grid fit to the complicated shape of the human body. Due to the computational complexities and uncertainties, some simplifications were added for example; infiltration and exfiltration were ignored in this work. Furthermore, the walls are assumed adiabatic.

Although some results of this study are compared with other studies. Still, some recommendations could be mentioned. For example, creating the same experimental model with the same boundary conditions would give a genuine validation, which could reveal the real findings. Therefore, it is recommended to create an experimental sample along with a simulation study.

In future studies, some work should be added. For instance, breathing spray and volatile particles should be used to be more accurately represented, giving better results and visualization. Furthermore, representing diffusers provided by a certain angle is also essential in either pollutant removal effectiveness or thermal comfort.

BIBLIOGRAPHIC REFERENCES

Abdel, K., & Saadeddin, R. (2016). *The Effects of Diffuser Exit Velocity and Distance Between Supply and Return Apertures on the Efficiency of an Air Distribution System in an Office Space*. https://openprairie.sdstate.edu/etd

Ahmed, T. (2012). Performance Investigation of Building Ventilation System by Calculating Comfort Criteria through HVAC Simulation. (*IOSR Journal of Mechanical and Civil Engineering*, *3*(6), 07–12). https://doi.org/10.9790/1684-0360712

Akili, Z. el, Bouzidi, Y., Merabtine, A., Polidori, G., & Chkeir, A. (2021). *Experimental Investigation of Adaptive Thermal Comfort in French Healthcare Buildings*. https://doi.org/10.3390/buildings11110551

Alhamid, M. I., Budihardjo, & Raymond, A. (2018). Design of the ventilation system and the simulation of air flow in the negative isolation room using FloVent 8.2. *AIP Conference Proceedings*, *1984*. https://doi.org/10.1063/1.5046600

Ameer, M., Azmi, A., Normunira, N., Hassan, M., & Salleh, Z. M. (2021). Investigation of Airflow in A Restaurant to Prevent COVID-19 Transmission Using CFD Software MALAYSIA *Corresponding Author Designation. *Progress in (Engineering Application and Technology*, *3*(1), 977–991). https://doi.org/10.30880/peat.2022.03.01.095

American Society of Heating, R. and A.-C. Engineers. (2012). *HVAC design manual for hospitals and clinics.*

Anthony, A. S., & Nath Verma, T. (2021). NUMERICAL ANALYSIS OF NATURAL CONVECTION IN A HEATED ROOM AND ITS IMPLICATION ON THERMAL COMFORT. (In *Journal of Thermal Engineering* (Vol. 7, Issue 1)). Yildiz Technical University Press.

Anuraghava, C., Abhiram, K., Naveen Sai Reddy, V., & Rajan, H. (2021). CFD modelling of airborne virus diffusion characteristics in a negative pressure room with mixed mode ventilation. *International Journal for Simulation and Multidisciplinary Design Optimization*, *12*. https://doi.org/10.1051/smdo/2021001

ASHRAE STANDARD. (2010). www.ashrae.org

Balocco, C., & Lio, P. (2011). Assessing ventilation system performance in isolation rooms. (*Energy and Buildings*, *43*(1), 246–252). https://doi.org/10.1016/j.enbuild.2010.09.020

Basse, N. T. (2019). *Turbulence Intensity Scaling: A Fugue*. https://doi.org/10.3390/fluids11205842

Baylar, A., Cihan Aydin, M., Unsal, M., & Ozkan, F. (2009). NUMERICAL MODELING OF VENTURI FLOWS FOR DETERMINING AIR INJECTION RATES USING FLUENT V6.2. (In *Mathematical and Computational Applications* (Vol. 14, Issue 2)).

Berlanga, F. A., Olmedo, I., de Adana, M. R., Villafruela, J. M., José, J. F. S., & Castro, F. (2018). Experimental assessment of different mixing air ventilation systems on ventilation performance and exposure to exhaled contaminants in hospital rooms. (*Energy and Buildings*, *177*, 207–219). https://doi.org/10.1016/j.enbuild.2018.07.053

Bolashikov, Z. D., Melikov, A. K., Kierat, W., Popioek, Z., & Brand, M. (2012). Exposure of health care workers and occupants to coughed airborne pathogens in

a double-bed hospital patient room with overhead mixing ventilation. (*HVAC and R Research*, *18*(4), 602–615). https://doi.org/10.1080/10789669.2012.682692

Borowski, M., Łuczak, R., Halibart, J., Zwolińska, K., & Karch, M. (2021). Airflow fluctuation from linear diffusers in an office building: The thermal comfort analysis. (*Energies*, *14*(16)). https://doi.org/10.3390/en14164808

Borro, L., Mazzei, L., Raponi, M., Piscitelli, P., Miani, A., & Secinaro, A. (2021). The role of air conditioning in the diffusion of Sars-CoV-2 in indoor environments: A first computational fluid dynamic model, based on investigations performed at the Vatican State Children's hospital. (*Environmental Research*, *193)*. https://doi.org/10.1016/j.envres.2020.110343

Cao, G., Ruponen, M., Paavilainen, R., & Kurnitski, J. (2011). Modelling and simulation of the near-wall velocity of a turbulent ceiling attached plane jet after its impingement with the corner. (*Building and Environment*, *46*(2), 489–500). https://doi.org/10.1016/j.buildenv.2010.08.012

Cehlin, M., & Moshfegh, B. (2010). Numerical modeling of a complex diffuser in a room with displacement ventilation. (*Building and Environment*, *45*(10), 2240–2252). https://doi.org/10.1016/j.buildenv.2010.04.008

Cheng, Z., Aganovic, A., Cao, G., & Bu, Z. (2021). *Experimental and simulated evaluations of airborne contaminant exposure in a room with a modified localized laminar airflow system*. https://doi.org/10.1007/s11356-021-12685-4/Published

Cho. (2019). Investigation on the contaminant distribution with improved ventilation system in hospital isolation rooms: Effect of supply and exhaust air diffuser configurations. (*Applied Thermal Engineering*, *148*, 208–218). https://doi.org/10.1016/j.applthermaleng.2018.11.023

Chow, T. T., Kwan, A., Lin, Z., & Bai, W. (2006). Conversion of operating theatre from positive to negative pressure environment. (*Journal of Hospital Infection*, *64*(4)), 371–378. https://doi.org/10.1016/j.jhin.2006.07.020

Croitoru, C. V., Nastase, I., & Bode, F. (2011). *AIR TURBULENCE INTENSITY INFLUENCE ON THE THERMAL COMFORT EVALUATION FOR DIFFERENT VENTILATION STRATEGIES*.

Çuhadaroğlu, B., & Sungurlu, C. (2015). *ID 8-A CFD analysis of air distributing performance of a New Type HVAC Diffuser*.

Daisey, J. M., Angell, W. J., & Apte, M. G. (2003). *INDOOR AIR QUALITY, VENTILATION AND HEALTH SYMPTOMS IN SCHOOLS: AN ANALYSIS OF EXISTING INFORMATION*.

Eldegwy, A. E. A., Khalil, E. E., Morcos, S. M., & Elbialy, E. M. (2015). Numerical investigations of indoor air quality in infection isolation rooms. (*13th International Energy Conversion Engineering Conference)*. https://doi.org/10.2514/6.2015-3820

Engineering Guide Air Distribution. (2011).

Gao, N., & Niu, J. (2006). Transient CFD simulation of the respiration process and inter-person exposure assessment. (*Building and Environment*, *41*(9), 1214–1222). https://doi.org/10.1016/j.buildenv.2005.05.014

Georges, L. (2017). *CFD simulation of active displacement ventilation Tollef Hjermann*.

Ghanta, N. (2020). *Meta-modeling and Optimization of Computational Fluid Dynamics (CFD) analysis in thermal comfort for energy-efficient Chilled Beams-based Heating, Ventilation and Air-Conditioning (HVAC) systems*.

Hallé. (2016). *PREDICTION OF BIOPARTICLES DISPERSION AND DISTRIBUTION IN A HOSPITAL ISOLATION ROOM*.

HVAC DESIGN MANUAL FOR HOSPITALS AND CLINICS. (2012).

Karimipanah, T., Awbi, H. B., & Moshfegh, B. (2012). *Evaluating the Performance of Air Distribution Systems in Enclosures*. https://www.researchgate.net/publication/344389593

Kekkonen *et al*. (2014). *Performance testing of engineering controls of airborne infection isolation rooms by tracer gas techniques _ Enhanced Reader*.

Ležovič, T., Lízal, F., Jedelský, J., & Jícha, M. (2013). HVAC automotive vents evaluation and their performance. (*HVAC and R Research*, *19*(8), 1073–1082). https://doi.org/10.1080/10789669.2013.824498

Liu, F., Zhang, C., Qian, H., Zheng, X., & Nielsen, P. v. (2019). Direct or indirect exposure of exhaled contaminants in stratified environments using an integral model of an expiratory jet. (*Indoor Air*, *29*(4), 591–603). https://doi.org/10.1111/ina.12563

Lu, Y., Oladokun, M., & Lin, Z. (2020). Reducing the exposure risk in hospital wards by applying stratum ventilation system. (*Building and Environment*, *183)*. https://doi.org/10.1016/j.buildenv.2020.107204

Mekbib Kifle, P. (2018). *CFD Simulation of heavily insulated office cubicle heated by ventilation air DONE IN COLLABORATION WITH*. www.oslomet.no

Mousavi. (2015). *AIRBORNE INFECTION IN HEALTHCARE ENVIRONMENTS: IMPLICATIONS TO HOSPITAL CORRIDOR DESIGN*. http://digitalcommons.unl.edu/constructiondisshttp://digitalcommons.unl.edu/constructiondiss/21

Mousavi & Grosskopf. (2014). Ventilation Rates and Airflow Pathways in Patient Rooms: A Case Study of Bioaerosol Containment and Removal. (*Annals of*

Occupational Hygiene, *59*(9), 1190–1199). https://doi.org/10.1093/annhyg/mev048

Novoselac_ASHRAE_Transactions_2003. (2003).

Prabhakaran, R. T. D., Curling, S. F., Spear, M., & Ormondroyd, G. A. (2018). *Simulation Model to Evaluate Human Comfort Factors for an Office in a Building*. 1126. https://doi.org/10.3390/proceedings2151126

Pulat, E., & Ersan, H. A. (2015). Numerical simulation of turbulent airflow in a ventilated room: Inlet turbulence parameters and solution multiplicity. (*Energy and Buildings*, *93*, 227–235). https://doi.org/10.1016/j.enbuild.2015.01.067

Risberg, D. (2018). *Daniel Risberg Analysis of the Thermal Indoor Climate with Computational Fluid Dynamics for Buildings in Sub-arctic Regions*.

Rusly, E., Airah, M., Gagliardini, S., & Australia, T. (2014). *The truth about the Air Diffusion Performance Index (ADPI)*.

SOLIDWORKS FLOW SIMULATION. (2021). *TECHNICAL REFERENCE SOLIDWORKS FLOW SIMULATION*.

Thatiparti, D. S., Ghia, U., & Mead, K. R. (2017). Computational fluid dynamics study on the influence of an alternate ventilation configuration on the possible flow path of infectious cough aerosols in a mock airborne infection isolation room. (*Science and Technology for the Built Environment*, *23*(2), 355–366). https://doi.org/10.1080/23744731.2016.1222212

Therkorn, J., Drewry, D., Pilholski, T., Shaw-Saliba, K., Bova, G., Maragakis, L. L., Garibaldi, B., & Sauer, L. (2019). Impact of air-handling system exhaust failure on dissemination pattern of simulant pathogen particles in a clinical biocontainment unit. (*Indoor Air*, *29*(1), 143–155). https://doi.org/10.1111/ina.12506

Thermal Environmental Conditions for Human Occupancy. (2004). www.ashrae.org

Tian, X., Zhang, S., Awbi, H. B., Liao, C., Cheng, Y., & Lin, Z. (2020). Multi-indicator evaluation on ventilation effectiveness of three ventilation methods: An experimental study. (*Building and Environment, 180)*. https://doi.org/10.1016/j.buildenv.2020.107015

Tsutsumi, J., Katayama, T.; & Hayashi, (2017). *NUMERICAL SIMULATION OF TURBULENT AIR FLOW IN A HOUSE INDUCED BY CROSS-VENTILATION)*.

TUTORIALS SOLIDWORKS FLOW SIMULATION 201. (2021).

Ventilation of Health Care Facilities. (2020). www.ashrae.org

Villafruela, J. M., Olmedo, I., Berlanga, F. A., & Ruiz de Adana, M. (2019). Assessment of displacement ventilation systems in airborne infection risk in hospital rooms. (*PLoS ONE*, *14*(1)). https://doi.org/10.1371/journal.pone.0211390

Yam, R., Yuen, P. L., Yung, R., & Choy, T. (2011). Rethinking hospital general ward ventilation design using computational fluid dynamics. (*Journal of Hospital Infection*, *77*(1), 31–36). https://doi.org/10.1016/j.jhin.2010.08.010

Yoon, S. H., Ahn, H. S., & Choi, Y. H. (2016). NUMERICAL STUDY TO EVALUATE THE CHARACTERISTICS OF HVAC-RELATED PARAMETERS TO REDUCE CO 2 CONCENTRATIONS IN CARS. (*International Journal of Automotive Technology*, *17*(6), 959–966). https://doi.org/10.1007/s12239−016−0093−y